Title
Arp2/3 Complex Activity Enables Nuclear YAP for Naïve Pluripotency of Human Embryonic Stem Cells

Author
Meyer, Nathaniel Paul

Publication Date
2023

Peer reviewed|Thesis/dissertation

Arp2/3 Complex Activity Enables Nuclear YAP for Naïve Pluripotency of Human Embryonic Stem Cells

by
Nathaniel Paul Meyer

DISSERTATION
Submitted in partial satisfaction of the requirements for degree of
DOCTOR OF PHILOSOPHY

in

Developmental and Stem Cell Biology

in the

GRADUATE DIVISION
of the
UNIVERSITY OF CALIFORNIA, SAN FRANCISCO

Approved:

DocuSigned by:
Todd Nystul
B55FB5CFA606452...

Todd Nystul
Chair

DocuSigned by:
Diane Barber

Diane Barber

DocuSigned by:
Wallace Marshall
43941FCFA7C0447...

Wallace Marshall

Committee Members

Dedicated to my sister for her unwavering support and love.

And secondly to my friends, colleagues, and mentors

who helped me never lose sight of my question.

Acknowledgements

Thank you to my supervisors Dr. Diane Barber and Dr. Todd Nystul for providing guidance and feedback throughout this project. Through all the meetings, discussions, presentations, data analysis – through all of it, both of you guided me and helped me develop as a scientist. I cannot thank you enough. To Diane, thank you for taking a chance on me, for believing in me, and for encouraging me. You created an environment which allowed me to grow as a thinker, as an educator, and as a scientist. I came to graduate school wanting to become the best scientist I could be – and you provided me the tools, the guidance, and the space to achieve that goal. Thank you. To Todd, thank you for helping me when I needed it most. Thank you for always being excited about my data and helping me find that excitement when I couldn't see it for myself. Thank you for inviting me into your lab, teaching me, and advocating for me. Thank you to the rest of my committee, Wallace Marshall, for your comments during committee meetings – your perspective was so helpful in shaping this project.

To Dr. Yi Liu – We spent so many hours in the tissue culture room together, talking, sharing, and laughing. You taught me to have resilience, you shared your culture with me, and you were always there when I needed help. Thank you for helping me sharpen my ideas, for helping me manage the workload of a research project, and for being a fantastic friend.

To my DSCB classmates and friends Dr. Arpana McKinney, Dr. Lauren Byrnes, and Dr. Steven Cincotta – thank you. I will never forget sitting in Mission Hall working on our qualifying exams, eating Cheez-It's while we discuss flaws in our experimental designs.

The three of you have never stopped supporting me, caring about me, and being my most vocal supporters throughout this entire process. A special thanks to Arpana, who stood with me as we finished this wild ride. We did it!

For the new friends who joined me in the final years of my PhD – Tania Singh, Lakyn Mayo, Kyle Jacobs, and Harnoor Virk. You are some of the most fantastic graduate students I have had the pleasure of working with, thank you for reminding me how exciting and passionate research can be. I am so excited for the future has in store for each of you. A special thank you to Harnoor Virk – your words of encouragement when I began to doubt what my career goals have stuck with me and will continue to motivate me for years to come.

Thank you to my lab mates – the Barbershop and the Nystulites. You all made me feel welcome, wanted, and appreciated. Thank you for teaching me and supporting me. A special thank you to Dr. Matthew Kutys and his lab – you helped me learn mechanical biology and put up with my endless questions!

Thank you to my mentor, Gerhard Bauer, who gave me the best piece of advice. You helped me decide which PhD program to accept and reminded me that I should always leave space in my world for happiness to be just as important.

Thank you to my friend Dr. Rebecca Jaszczak. We became friends in the most serendipitous of ways and I am so thankful for that shuttle ride back from "3rd Year Reorientation™". You have supported me, encouraged me, and been an ally in this battle. From sharing our nerdy hobbies, to discussing inane science issues, to spending a stupid amount of time deciding what we were in the mood to eat for lunch – you were always

there and always willing to help. You shared your life with me and I cannot thank you enough. Thank you for being one of my best friends.

Thank you to my sister, Cassandra Meyer. Over ten years ago, you drove me through the woods for six hours to drop me off at college. Realizing how cold it was, you gave me one of your blankets – one you had in your car for emergencies – just to make sure I had something to keep me warm while I studied. I sit here now, finishing this dissertation, over a decade later, wrapped in that very same blanket. You have been my champion, my supporter, my friend, and the best big sister in the world. You have been my sounding board, listening to my crazy science ideas for longer than anyone should have to put up with. Yet, just a moment ago, completely out of the blue, you messaged me asking about the role of Wnt in stem cell de-differentiation and regeneration. I appreciate you so much, for all that you have given me and continue to give me. I know that you will be such a big part of my future, you have already shaped so much of who I am.

Thank you to my brother, Alexander Meyer. I think back to how Mom describes our relationship – we went from constantly fighting, arguing, bickering, to waking up one day and being best friends. I knew from then on you would always have my back and would always, always, always help me whenever you could. And you have, through all these years, you have supported me, encouraged me, and allowed me to be me. From listening to me rant on the phone for hours about whatever exam or experiment or idea I had on my mind at the time, to times we spoke on the phone actively *not* talking about those things when I needed space away. You encouraged me to be balanced, to find other interests, and to not let the stress of life get to me. Thank you for being my brother. And

a special thank you to Milo, Benji, and Ellie – you're the best nephews and niece in the world!

Thank you to my mother, Diane Meyer. I know that raising me wasn't always the easiest – I never stopped asking you questions, never stopped wondering about the world around me, and always turned to you for the answer to everything. In spite of how annoying I am sure that was, you always encouraged me. You taught me where and how to find the answers on my own and shared the joy with me as I talked incessantly about what I learned. You also encouraged me to be balanced, to never let me stop my musical interests, and to make sure that I made space in my life for other interests. Thank you for being my mom. I love you.

Thank you to my friends Amanda Bouldin, Christopher Minor, and Keith Wade for constantly taking me on adventures – they were much needed breaks from lab. From random messages with crazy jokes, to phone calls while driving home from lab, the three of you were my reminders to enjoy life and take breaks from science. Thank you.

Thank you to my priest Russell Williamson, M.Div, for your spiritual guidance. You have been with me throughout this entire process, and have been nothing but accepting, loving, and supportive. Thank you.

Thank you to my friends Dr. Natanya Kerper, Dr. Marc Meadows, Dr. Daniel Bunis, Dr. Ashley Libby, Dr. Sumitra Tatapudy, Dr. Katja Rust, Dr. Katie White, Dr. Ellen Kettler, Tawny Neal, Hanna Kirby, Shannon Weaver, Dr. Akela Kuwahara, Dr. Daniel Wong, Dr. Mark Sherman, Dr. Dan Holohan, and Hal Doan.

And lastly, thank you to my partner, Robert Rushing, for being my rock and for loving me. You have taught me so much about so many things; I could not have done this without

you. Thank you for your patience – from reminding me to eat, encouraging me to go to bed, to standing by me as I finish this PhD. From helping me navigate complex decisions, to sharing funny videos of dogs to make me laugh – you have been the brightest light in my life from the moment we met. I truly cannot imagine what this journey could have been like without you. Thank you for giving me a place of safety and love, so that I could conquer my PhD and beyond. I love you the mostest. I win.

Contributions

The work in this dissertation was performed under the direct supervision of Dr. Diane Barber, Ph.D and Dr. Todd Nystul, Ph.D. Further guidance and valuable insight came from thesis committee member Dr. Wallace Marshall, Ph.D.

Chapter 2 of this work is adapted from efforts described in a submitted manuscript

Nathaniel Paul Meyer, Todd Nystul, and Diane Barber. “Arp2/3 Complex Activity Enables Nuclear YAP for Naïve Pluripotency of Human Embryonic Stem Cells.” *In review*.

Chapter 3 of this work, in part, is adapted from a collaborative effort with Todd Nystul’s lab as it appears in the following publication:

Nathaniel Paul Meyer*, Jobelle Peralta*, and Todd Nystul. “Preparation of Drosophila Ovarioles for Single-Cell RNA Sequencing.” Methods in Molecular Biology. *In press*.

* authors contributed equally to this work

Dinanzi a me non fuor cose create
se non etterne, e io etterno duro.
Lasciate ogne speranza, voi ch'intrate'

– Dante Alighieri, La Divina Commedia

Arp2/3 Complex Activity Enables Nuclear YAP

for Naïve Pluripotency of Human Embryonic Stem Cells

Nathaniel Paul Meyer

Abstract

Despite current understanding of transcriptional and epigenetic programs regulating transitions of human embryonic stem cells between distinct stages of pluripotency, our knowledge of the cell biology of changes in pluripotency states remains limited. We report a dynamic remodeling of the actin cytoskeleton of human embryonic stem cells (hESCs) as they transition from primed to naïve pluripotency that includes assembly of a ring of contractile actin filaments encapsulating colonies of naïve hESCs. The actin ring requires activity of the Arp2/3 complex and traction force microscopy suggests a role in limiting cell-substrate tensional forces. Arp2/3 complex activity is also necessary for effective transition to the naïve pluripotency state, including translocation of the Hippo pathway effectors YAP and TAZ from the cytosol to the nucleus. In hESCs with inhibited Arp2/3 complex activity, expressing a nuclear-localized YAP-S127A restores assembly of the actin ring and the naïve pluripotency state, including established markers and colony formation. Together these new findings on the cell biology of hESC reveal a signaling network of Arp2/3 complex activity for dynamic remodeling of contractile actin filaments and YAP/TAZ activity for transition to the naïve pluripotency state.

Table of Contents

List of Figures

List of Tables

Chapter 1 – The Cytoskeleton and Human Naïve Pluripotency

1.1 – Primed and Naïve Pluripotency

Derivation of clonal pluripotent stem cells (PSCs) from embryos yields cells with a spectrum of pluripotent states, dependent on developmental progression of the embryo, species, and culture condition. Clonal mouse embryonic stem cells (mESCs) represent a ground-state of pluripotency and closely recapitulate the naïve blastocyst from which they are isolated (Nichols & Smith, 2009). In contrast, clonal human and other primate PSCs, as conventionally isolated and maintained, exist in a primed state of pluripotency and more closely resemble the post-implantation epiblast (Nakamura et al., 2016). Importantly, naïve pluripotent stem cells retain characteristics of the inner cell mass, such as the ability to contribute to chimera formation including germ cells and dual active X-chromosomes (Hanna et al., 2009). To study the naïve state of clonal human PSCs, culture conditions were developed that dedifferentiate primed human embryonic stem cells (hESCs) to a naïve state of pluripotency (Duggal et al., 2015; Szczerbinska et al., 2019; Takashima et al., 2014a; Theunissen et al., 2014). Development of culture conditions that convert and sustain a naïve pluripotent state in human PSCs, which retain characteristics of the pre-implantation blastocyst, has provided an opportunity to study human development before gastrulation (Rossant & Tam, 2017).

Utilizing these culture conditions, extensive studies have interrogated the transcriptional regulatory network that controls the switch between naïve and primed pluripotency in both human and mouse (Li & Belmonte, 2017; Weinberger et al., 2016). A number of pluripotency transcription factors have been identified in these studies, which sustain a cascade of regulatory events constituting a core gene regulatory network that

maintains the pluripotency status seen in both the naïve and primed states (Ng & Surani, 2011). These core pluripotency factors include the conventional Yamanaka factors OCT4, SOX2, and NANOG, among others (Masui et al., 2007; Niwa et al., 2000). Through many global transcriptome analyses of both *in vitro* models of naïve pluripotency as well as human embryos, transcriptional signatures of human naïve pluripotency have been established which highlight KLF4, KLF17, ESRRB, and OTX2 as important markers of the human naïve state (Collier & Rugg-Gunn, 2018). Notably, specific transcription factors enriched in naive hESCs such as KLF4 and TFCP2L1 are sensitive to perturbation only in naïve hESCs, implying that a unique rewiring of the core pluripotency network occurs during transition to the naïve state (Takashima et al., 2014b). Despite these extensive studies, the transcriptomic heterogeneity of both naïve and primed hESCs has remained a primary focus within the field as methods used to generate, culture, and analyze pluripotent hESCs are found to markedly impact differences in gene expression (Messmer et al., 2019). Additionally, how other factors may influence pluripotency gene expression such as differences in the mechanical environment including cytoskeletal remodeling, mechanosensing, and cell-cell dynamics within hESC colonies remain poorly understood.

1.2 – Arp2/3 Complex Activity and Actin Architectures in hESCs

The *in vitro* models of naïve pluripotency have provided insights on the transcriptomic, epigenetic, and proteomic programs stem cells maintain for a functional naïve pluripotency state (Duggal et al., 2015; Theunissen et al., 2016; Warrier et al.,

2017). We have limited understanding, however, of how established morphological changes during the transit from primed to naive states are regulated and whether morphological changes regulate state transitions. We do know that pluripotent stem cell fate is intricately regulated by biophysical cues transmitted through the actin cytoskeleton, which control gene expression, proliferation, and differentiation (Naqvi & McNamara, 2020), and that coordinated changes in cell shape mediated by the actin cytoskeleton are essential for developmental embryogenesis (Chalut & Paluch, 2016). Consequently, mechanoregulation has been studied for roles in exit of the pluripotent state toward targeted cell fates including endodermal (Y. F. Chen et al., 2020), ectodermal (Keung et al., 2012), and mesodermal (Przybyla et al., 2016) lineages (Ireland & Simmons, 2015). Directly targeting actin filament dynamics has also been shown to regulate the pluripotent fate of stem cells (Gerecht et al., 2007; Hogrebe et al., 2020; Rosowski et al., 2015a).

Actin filament remodeling is established to drive changes in cell shape associated with myriad cell behaviors, including motility, proliferation, and adherens junctions dynamics (Chhabra & Higgs, 2007; Goley & Welch, 2006; May, 2001). Actin filament architectures are predominantly generated by two classes of actin nucleators – the Arp2/3 complex and the formins. The Arp2/3 complex comprises of seven subunits which nucleate branched actin filaments, whereas the formins, a family of fifteen mammalian isoforms, nucleate unbranched filaments. Actin filament nucleation is energetically unfavorable and these assembly factors overcome this barrier to facilitate dynamic cytoskeletal architectures and complex cell behaviors (Chhabra & Higgs, 2007). Each class of assembly factors are regulated by distinct mechanisms including mechanical

stimuli or signaling pathway stimulation and inhibition. Arp2/3 complex activity is critical for regulation of cellular and tissue mechanics including contractility, membrane stiffness and membrane tension (Papalazarou & Machesky, 2021). As such, Arp2/3 complex-dependent actin remodeling lies at a critical interface between the cell and the microenvironment by mediating transmission of biological, chemical, and mechanical stimuli from the environment, including neighboring cells, to the cell interior. Despite this, the role of Arp2/3 complex activity, actin remodeling, and how those components regulate actin-associated proteins in human ESCs has remain understudied.

Actin-associated proteins, including β-catenin for enabling Wnt pathway activity and ezrin-radixin-moesin (ERM) proteins for enabling tensional forces at the plasma membrane, facilitate maintenance of the naïve pluripotent state in mESCs (de Belly et al., 2021b). During murine preimplantation development, actin filaments generate mechanical forces that contribute to differentiation throughout the blastocyst stage by modulating mechanosensitive signaling pathways such as Hippo signaling (Hirate et al., 2015; Zenker et al., 2018). These actin structures allow cells within the developing blastocyst to organize based on contractility, coupling mechanosensing and fate specification (Maître et al., 2016). Despite evidence that morphological changes and actin filament remodeling determine naïve pluripotency during mouse development, their roles in human naïve pluripotency remain unknown.

1.3 – Physical Forces and Pluripotency

Actin filament dynamics can be regulated by the mechanical microenvironment and transmit tensional signals to the cell interior (Janmey & McCulloch, 2007). Homeostasis of tension in response to mechanical forces is achieved in part by regulating focal adhesion assembly and disassembly and through regulating the underlying cytoskeletal structure through actomyosin contractility (Vining & Mooney, 2017). These changes in the actin cytoskeleton ultimately exert forces on the cell membrane and lead to changes in cell shape; thus, cell shape and the cytoskeleton are direct readouts of cell mechanics (Clark et al., 2014). Several studies have linked changes in cell shape to changes in cell signaling, transcriptional activity, and cell fate. For example, epidermal stem cell differentiation is regulated by actin polymerization controlling serum response factor signaling (Connelly et al., 2010). Additionally, changes in cell shape of mESCs regulate STAT3 signaling and self-renewal (Murray et al., 2013). Understanding how PSCs sense, interpret, and react to changes in their mechanical environment are thus vital to understanding stem cell biology.

However, the use of mESCs for studying how mechanical stimuli interact with changes in cell fate and pluripotency has significant limitations. In mice, the first cell fate decision during blastomere compaction is resolved by Hippo signaling activity, a pathway known to be regulated by mechanical forces. The Hippo effector proteins YAP and TAZ repress naïve identity and promote trophectoderm differentiation in the developing blastomere (Frum et al., 2018). The signaling requirements to induce exit from naïve pluripotency were established and found to be largely driven by fibroblast growth factor

(FGF) and extracellular signal-regulated kinase (ERK) signaling (Kunath et al., 2007; Nett et al., 2018). Additionally, as mESCs exit the naïve state and differentiate, they display a striking remodeling of the actin cytoskeleton and changes in cell shape indicative of a change in cell mechanics (Aloisio & Barber, 2022; Chalut & Paluch, 2016). However, when naïve mESCs were directly stimulated mechanically, they were found to be extremely limited in their mechanoresponsitivity. Although minor acute cellular changes were observed, stimulated mESCs were found to be indistinguishable from unstimulated mESCs transcriptionally; only after exiting naïve pluripotency did mESCs alter their transcriptional response under mechanical stimulation (Verstreken et al., 2019). These data suggest that although mESCs remodel their cytoskeleton, regulate their transcriptional activity, and dynamically transition between states of pluripotency, these processes may be less directly regulated by mechanical stimuli than initially thought. In support of this, many of these processes are regulated by mechanically independent mechanisms. For example, YAP and TAZ can be regulated by adherens junctional and tight junctional sequestration independent of mechanical stimuli (Nishio et al., 2015).

Unlike mESCs, human ESCs do appear to be mechanically sensitive and respond transcriptionally yet come with their own limitations for use as a model to interrogate mechanics, cell fate, and signaling. Unlike mESCs, hESCs are conventionally cultured in the primed state and thus studying pluripotency dynamics requires dedifferentiation to naïve pluripotency. Consistent with mESCs that have exited the naïve state, primed hESCs are known to be highly mechanoresponsive including changing cell shape, cytoskeletal dynamics including contractility, and their transcriptome in response to

mechanical stimuli (Y. Sun et al., 2012). However, upon dedifferentiation to a naïve state of pluripotency, hESCs were found to be mechanoresponsive with changes in the mechanical environment such as matrix stiffness and 3D culture conditions found to promote self-renewal and maintenance of the naïve state (McKee et al., 2021). In particular, maintaining naïve hESCs in different mechanical environments facilitates expression of genes such as FLNC, COL4, CAV1, SERPINE1, and AKT1, which have all been associated with integrin-mediated focal adhesion remodeling or actin cytoskeletal remodeling (Mair et al., 2019; Wrighton et al., 2014). Activation of integrin receptors stimulates PI3K/Akt signaling, which functions as an inhibitor of the ERK signaling pathway (Singh et al., 2012). Activation of Akt signaling alone is sufficient to maintain pluripotency in both mouse and human ESCs, playing an essential role in downstream regulation of STAT, ERK, and β-catenin signaling (Watanabe et al., 2006). Thus, hESCs represent a tractable model system to study the role of mechanical signaling in the context of cell shape changes, cell fate transition, and pluripotency. However, how responses to mechanical stimuli ultimately lead to changes in the dynamic pluripotency networks used to establish naïve or primed pluripotency remains unclear.

1.4 – YAP, Hippo Signaling, and Pluripotency

Changes in cell shape induced by mechanical stimuli often regulated by Rho GTPases and promote translocation of mechanosensitive transcription factors such as Yes-associated protein (YAP) in human ESCs (Hoon et al., 2016; Hsiao et al., 2016a). YAP and its transcriptional co-activator WW domain containing-transcription factor 1 (WWTR1 or TAZ) are effector proteins for the Hippo signaling pathway (Plouffe et al.,

2018). Much work has gone into understanding the role of Hippo signaling both developmentally as well as in *in vitro* models of human pluripotency, with Hippo signaling now recognized as a major regulator of stem cell pluripotency, but often with pleiotropic and context-dependent effects (Mo et al., 2014).

For instance, Hippo signaling is highly regulated in primed mESCs, leading to the exclusion of YAP/TAZ from the nucleus (Nishioka et al., 2009b). Conversely, depletion of YAP/TAZ from naïve mESCs enhances resistance to differentiation and reinforced the naïve pluripotent state (Azzolin et al., 2014). The divergent roles of YAP/TAZ in mouse suggest that Hippo pathway function may act as a regulator of naïve and primed pluripotency status. This was recently confirmed for hESC whereupon YAP overexpression in primed hESCs promoted long-term survival and expansion of hESCs as well as facilitated dedifferentiation to naïve pluripotency (Ohgushi et al., 2015; Qin et al., 2016). These studies used both genetic and pharmacological approaches, including supplementing the culture medium with lysophosphatidic acid, which inhibits Hippo signaling and promotes nuclear YAP localization. Inhibiting YAP with Verteporfin markedly decreases expression of both core pluripotency markers as well as naïve pluripotency markers in naïve hESCs (McKee et al., 2019). Although mechanosensitive signaling pathways play an important role in the regulation of pluripotency states, the molecular machinery that regulates these pathways remains poorly understood.

1.5 – Chapter Conclusion

Despite the recognized and substantial differences in cell morphology of distinct ESC pluripotency states (Tatapudy et al., 2017), we have a limited understanding of what regulates these distinct morphologies and whether they contribute to determining a pluripotent state. Embryonic stem cells are responsible for ultimately giving rise to every cell in the adult organism. To achieve this complexity, a wide-ranging and diverse series of cellular events occur between the first cell divisions, first cell fate specification, and the final terminal differentiation to a somatic cell type. Studying the mechanisms and methods of how cells navigate these changes will continue to be a fundamentally significant and clinically relevant area of study.

As cells navigate changes in cell fate, many components of the cell change, including cell morphology. The role of mediators of cell morphology such as actin nucleators remains unknown in hESCs. A plethora of cytoskeletal components are known to facilitate many of these cell fate decisions, with actin dynamics itself playing vital and necessary roles in many of them. Interrogating how the environment communicates through the cytoskeleton to the cell interior to inform how, when, where, and why changes in cell shape, fate, and behavior occur are key to deepening our understanding of pluripotency. The divergent roles of mechanosensitive signaling pathways such as Hippo when comparing mouse and human underscore the importance of studying human biology for careful characterization of human pluripotency. The role of the actin cytoskeleton in human pluripotency, including the role of actin nucleators, actin architectures, physical forces, and mechanosensing remains unclear. Understanding the

mechanisms behind how and why these differences exist will facilitate optimization of downstream applications for human pluripotent stem cells.

My thesis work addresses these questions by characterizing the role of cytoskeletal dynamics and remodeling in hESCs. We identified the assembly of a ring of contractile actin filaments encapsulating naïve but not primed colonies that is tethered to adherens junctions and decorated with phosphorylated myosin light chain (pMLC) and moesin. We found that nucleating activity of the Arp2/3 complex but not formins is necessary for the actin ring, naïve cell mechanics, including decreased cell-substrate tensional forces and colony formation, and transition to naïve pluripotency. RNAseq analysis revealed a role for Hippo pathway signaling in Arp2/3 regulated naïve pluripotency, which we confirmed by showing increased nuclear localization of the transcriptional co-activators YAP and TAZ in naïve compared with primed hESCs that is blocked by inhibiting Arp2/3 complex activity. Consistent with these findings, naïve pluripotency that is blocked with inhibiting Arp2/3 complex activity is restored by expressing a nuclear-localized non-phosphorylatable YAP (YAP-S127A) (Zhao et al., 2007). These data provide new mechanistic insights on how actin filament dynamics regulates the naïve state of hESCs pluripotency and the integration between actin filament remodeling and pluripotency.

Chapter 2 – Arp2/3 Complex Activity Enables Nuclear YAP for Naïve Pluripotency of Human Embryonic Stem Cells

2.1 – Actin Filament Remodeling as hESCs Transition to a Naïve State

For morphological analysis of pluripotency states, HUES8 primed hESCs were grown on Matrigel and dedifferentiated to naïve pluripotency using previously reported conditions in an mTeSR-based medium supplemented with ERK (PD0325901) and GSK3 (CHIR99021) inhibitors, the adenylyl cyclase activator forskolin, human leukemia inhibitory factor (LIF), basic fibroblast growth factor (bFGF), and ascorbic acid (Duggal et al., 2015; Qin et al., 2016). We confirmed transition to a naïve state by showing that colonies have prominent doming by day 6 of dedifferentiation and increased expression of pluripotency markers DNMT3L, DPPA3, KLF2, and KLF4, as determined by rt-PCR (**Fig. 2.1 A-B**). Staining fixed cells for actin filaments with phalloidin revealed that naïve but not primed colonies had a ring of bundled actin filaments at the colony periphery (**Fig. 2.1 C**). These supracellular actin rings also formed around colonies of naïve H9 cells and naïve WTC11 iPSCs (**Fig 2.5 A**) as well as HUES8 cells dedifferentiated by alternative medium supplements (**Fig. 2.5 B**). Moreover, the actin ring assembled independently of naïve colony size (**Fig. 2.5 C**).

A similar actin ring is reported to encircle colonies of clonal human pluripotent stem cells to provide a mechanosensitive element linked to focal adhesions (Närvä et al., 2017). The actin filament ring we observed around naïve hESC colonies was instead tethered to adherens junctions, as indicated by co-labeling for β-catenin, with separated interdigitated adherens junctions suggesting a contractile force (**Fig. 2.1 D, crosshairs**). The contractile property of the ring was also suggested by the actin ring being decorated with pMLC as determined by immunolabeling (**Fig. 2.1 E**). In contrast, primed hESC

colonies had irregular aggregates of pMLC with limited co-localization with actin filaments. Immunolabeling with pan-ERM antibodies showed co-localization with the actin filament ring in naïve cells, and ERM-specific antibodies revealed co-localization of moesin but not ezrin or radixin (**Fig. 2.1 F, Fig. 2.5 D**). Together, these data indicate a contractile actin ring surrounding naïve but not primed hESC colonies.

The supracellular nature of the actin ring and differential pMLC labeling between naïve but not primed hESC colonies suggested a potential difference in colony mechanics, which we determined by using traction force microscopy. Increased cell-matrix traction forces are associated with destabilized adherens junctions in epithelial monolayers (Mertz et al., 2013; Scarpa et al., 2015). Consistent with pMLC localization, primed colonies exhibited elevated cell-substrate tractions that were distributed throughout the colony (**Fig. 2.1 G, left**). In contrast, naïve colonies exhibited overall low magnitude cell-substrate tractions that were localized to the colony periphery and largely absent from the colony interior (**Fig. 2.1 G, right**), suggesting decreased cell-substrate tensional force and a likely shift to more stabilized cell-cell forces. Along with pMLC localization, these low tractions are consistent with uniform cell-cell adhesion in naïve hESC colonies. Together these data identify a significant reorganization of the actin cytoskeleton during transition to a naïve state of pluripotency that includes the assembly of a contractile actin ring surrounding naïve cell colonies, coincident with attenuated cell-substrate traction forces and a transition to enhanced cell-cell junction traction force within the colony unit.

2.2 – Arp2/3 Complex Activity is Necessary for Transition of hESC to Naïve Pluripotency

The assembly of an actin ring in naïve but not primed hESC colonies led us to ask whether the actin ring has a functional significance in the transition to naïve pluripotency. New actin filaments are predominantly generated by two distinct nucleators, the Arp2/3 complex, which generates branched filaments, and formins, which generate unbranched filaments (Pollard, 2007). We found that the actin ring assembled when naïve cells are generated in the presence of SMIFH2, a broad-spectrum inhibitor of formin activity (Ganguly et al., 2015; Rizvi et al., 2009) but not CK666, a selective pharmacological inhibitor of Arp2/3 complex activity (Nolen et al., 2009; Yang et al., 2012) (**Fig. 2.2 A**). Additionally, CK666 blocked increased expression of markers of naïve pluripotency seen in controls, determined by qPCR of PECAM1, ESRRB, KLF4, and DNMT3L (**Fig. 2.2 B**). To eliminate the possibility that CK666 led cells to exit pluripotency and differentiate, we immunolabeled for the general pluripotency markers OCT4 and SOX2 and found that CK666 treated cells remained broadly pluripotent (**Fig. 2.6**). To further assess the pluripotent state of cells dedifferentiated in the presence of CK666, we immunolabeled for the primed pluripotent marker SSEA3 (Trusler et al., 2017). In controls, SSEA3 expression significantly decreased with dedifferentiation, as previously reported (Liu et al., 2017) but not with CK666 (**Fig. 2.2 C, D**). Additionally, the naïve pluripotency marker KLF4 (Takashima et al., 2014c) translocated from the cytoplasm to the nucleus with control dedifferentiation but not in the presence of CK666 (**Fig. 2.2 C, E**).

We further tested for a functional naïve pluripotent state by staining for alkaline phosphatase (AKP) and scoring for colony formation, which indicates the capacity for clonogenic expansion and self-renewal (Rostovskaya et al., 2019). Primed and naïve hESCs were passaged and plated at clonogenic cell numbers and maintained for five days without or with CK666. In controls, colony formation was greater in naïve compared with primed hESC, as previously reported (Chen et al., 2022). However, with CK666, but not CK689, an inactive analog of CK666, there was no increase in colony formation in naïve compared with primed cells (**Fig. 2.2 F**). Additionally, traction force microscopy revealed that elevated cell-substrate tractions throughout colonies of primed but not naïve cells (**Fig. 2.1 G**) were retained when hESCs were dedifferentiated in the presence of CK666 (**Fig. 2.2 G**). These data identify an essential role for the Arp2/3 complex in promoting an actin filament ring and uniform naïve colony mechanics as well as acquiring a naïve pluripotent state in hESCs.

2.3 – Arp2/3 Complex Activity Enables Active YAP for Naïve Pluripotency

To understand how Arp2/3 complex activity affects the transcriptional circuitry required for naïve pluripotency, we performed bulk RNA-sequencing (RNAseq) on primed cells, naïve cells, and primed hESCs dedifferentiated in the presence of CK666 (**Fig. 2.3 A**). We found that primed, naïve, and CK666-treated cells had a total of 12,817 differentially expressed genes (DEGs) with an adjusted *pval <0.05*. Of these DEGs, 182 were unique to control primed cells compared with control naïve cells and were not

differentially expressed in CK666-treated cells; CK666-treated cells compared with control primed or control naïve cells had 102 and 502 DEGs, respectively. To determine the transcriptional networks involved in the dedifferentiation from primed to naïve pluripotency, we identified KEGG pathways in control naïve dedifferentiation that revealed Hippo signaling as the top candidate (**Fig. 2.3 B**). Additionally, transcription factor binding motif analysis identified TEAD2 as a top candidate, which is a downstream effector of Hippo signaling (**Fig. 2.3 C**).

The Hippo effector protein YAP is a known regulator of the human naïve pluripotent state, with overexpression of YAP in pluripotent stem cells promoting the acquisition of naïve pluripotency (Qin et al., 2016). Although actin filament dynamics, including a contractile ring of actin, regulate YAP signaling (Furukawa et al., 2017; Hsiao et al., 2016b), to our knowledge a role for Arp2/3 complex activity regulating YAP or TAZ activity in human naïve pluripotency has not been reported. For an unbiased global analysis of known YAP target genes, we used two publicly available datasets (Estarás et al., 2017; Pagliari et al., 2021) and found that of the 3,744 YAP target genes identified in our RNAseq dataset, 3156 (84%) were not differentially expressed in any condition and 588 (16%) were enriched in one or multiple conditions. Of those 588 enriched YAP-target genes, 174 (30%) were significantly enriched in the control naïve dedifferentiation condition versus the control primed condition; 407 (69%) were significantly enriched among CK666-treated dedifferentiation condition versus the control primed condition; and 7 (1%) were significantly enriched in both conditions versus the control primed condition (**Fig. 2.3 D**, adjusted pval >0.05).

Of the genes significantly enriched in the control naïve condition compared with the control primed condition, known naïve pluripotency markers such as OTX2, DLG2, and CRY1 were significantly upregulated; these naïve markers failed to significantly increase in the CK666-treated condition (**Fig 2.3 E, left**). As expected, genes significantly enriched among both DEG lists include known YAP and Hippo targets such as ANKRD1, SLIT2, and CHD10. (**Fig. 2.3 E, right**). Genes significantly enriched among the CK666-treated condition include the negative Hippo regulator AMOT (Zhao et al., 2011), and lineage-commitment genes such as SOX6 and SPEF2 (**Fig. 2.3 E, middle**). These data suggested a Hippo signaling pathway program, driven by mediators such as YAP, occurs during dedifferentiation to naïve pluripotency but is disrupted by inhibiting Arp2/3-complex activity. To verify this prediction, we immunolabeled cells to determine YAP localization and found increased nuclear to cytoplasmic ratios of YAP (**Fig. 2.3 F-G**) and TAZ (**Fig. 2.6**) with control dedifferentiation that was blocked by CK666.

Consistent with these data, during preimplantation development, actin filaments and associated proteins generate mechanical forces that contribute to differentiation throughout the blastocyst stage through modulation of mechanosensitive pathways such as Hippo signaling (Hirate et al., 2015; Zenker et al., 2018). These actin structures allow cells within the developing blastocyst to organize based on contractility, coupling mechanosensing and fate specification (Maître et al., 2016). Therefore, we hypothesized that Arp2/3 complex activity facilitated naïve dedifferentiation through increasing YAP nuclear localization. To test this prediction, we asked whether primed hESCs stably expressing a constitutively active, nuclear-localized form of YAP (YAP-S127A) could

restore naïve dedifferentiation in the presence of CK666. Accordingly, we observed that two immunofluorescence-based markers of the naïve state, increased nuclear localization of KLF4 (**Fig. 2.4 A-B**) and decreased SSEA3 (**Fig. 2.4 C-D**), were rescued by overexpression YAP-S127A in the presence of CK666. In contrast, acquisition of a naïve state of pluripotency remained blocked with CK666 treatment in cells overexpressing wildtype YAP (WT YAP) (**Fig. 2.4 A-D**). Additionally, YAP-S127A rescued colony formation, a functional form of naïve pluripotency, that was inhibited with CK666 (**Fig. 2.4 E**).

2.4 – Chapter Conclusion

Our new findings support a model in which naïve pluripotency is characterized by an Arp2/3 complex-dependent remodeling of the actin cytoskeleton that includes formation of a contractile supracellular actin ring enclosing naïve colonies and establishment of uniformity in colony mechanics likely enabled by the actin ring being physically associated with β-catenin and moesin, which are known to play roles in pluripotency (de Belly et al., 2021a; Xu et al., 2016) (**Fig. 2.4 F**). Moreover, Arp2/3 activity facilitates dedifferentiation to a naïve state of pluripotency through promoting nuclear translocation of YAP and regulating Hippo target gene expression. Consistent with these findings, naïve pluripotency that is blocked with inhibited Arp2/3 complex activity is restored by expressing a constitutively active, nuclear-localized YAP-S127A.

Our findings are distinct from those on a contractile actin filament ring that assembles around colonies of primed pluripotent stem cells (Närvä et al., 2017) and Xenopus neural crest cells (Shellard et al., 2018), which functions to enhance cell-

substrate adhesion and migratory capacity, respectively. Our findings also highlight distinct differences between murine and human embryonic stem cells. Cells within the ICM of mouse blastocysts exclude YAP from the nucleus whereas cells within the ICM of human blastocysts maintain nuclear YAP (Nishioka et al., 2009; Qin et al., 2016). This difference in YAP localization is retained *in vitro*, with murine naïve PSCs having predominantly cytosolic YAP (Chung et al., 2016), and human naïve PSCs having predominantly nuclear YAP (**Fig. 2.3 F-G**). How this difference in YAP localization occurs between mouse and human is unknown, although a number of cytoskeletal factors regulate YAP localization, including stability of the actin cytoskeleton, contractility, and mechanical regulators such as ERM proteins (Furukawa et al., 2017). The role of the actin cytoskeleton in the exit from the pluripotent state has also highlighted how actin dynamics may facilitate cell fate decisions. For example, cells located at the colony edge of primed hESCs have distinct cytoskeletal dynamics and are uniquely poised to exit pluripotency and differentiate (Kim et al., 2022; Rosowski et al., 2015b). Positional differences in differentiation potential such as these have been proposed as a mechanism executed in early embryo symmetry breaking with rearrangement of the actin cytoskeleton being required for the first cell fate decision in the blastocyst (Q. Chen et al., 2018; Skamagki et al., 2013). Thus, it may be possible that the contractile actin ring we observe at the edge of naïve colonies (**Fig 2.1 C**) functions as a hub for regulating cell fate dynamics through similar mechanisms as first cell fate decision including modulation of mechanosensitive signaling such as YAP and through pathways such as Hippo.

Further highlighting differences between human and mouse ESCs, we recently reported that Arp2/3 complex activity is necessary for the differentiation of clonal mouse naïve ESCs to the primed epiblast state, which is in part mediated by translocation of myocardin-related transcription factor MRTF from the cytosol to the nucleus (Aloisio & Barber, 2022). Additionally, a recent report suggests that Arp2/3 complex activity may form a positive feedback loop with YAP-TEAD1 transcriptional activity controlling cytoskeletal reorganization (Pagliari et al., 2020); thus Arp2/3 complex activity may regulate naïve pluripotency at multiple stages including initially to reorganize the actin cytoskeleton, but also during maintenance of naïve pluripotency through regulating YAP localization and hence activity.

Our findings increase our understanding of actin dynamics and cell mechanics as regulators of cell fate transitions. A role for contractile actin filaments as a mechanoresponsive element for pluripotency states is well established (de Belly et al., 2022), and our work identifies cytoskeletal dynamics essential for uniform colony mechanics and the naïve pluripotent state, the role of Arp2/3 complex activity, and YAP/TAZ activity as a promising target for reprogramming of hESCs and for regenerative medicine.

2.5 – Figures

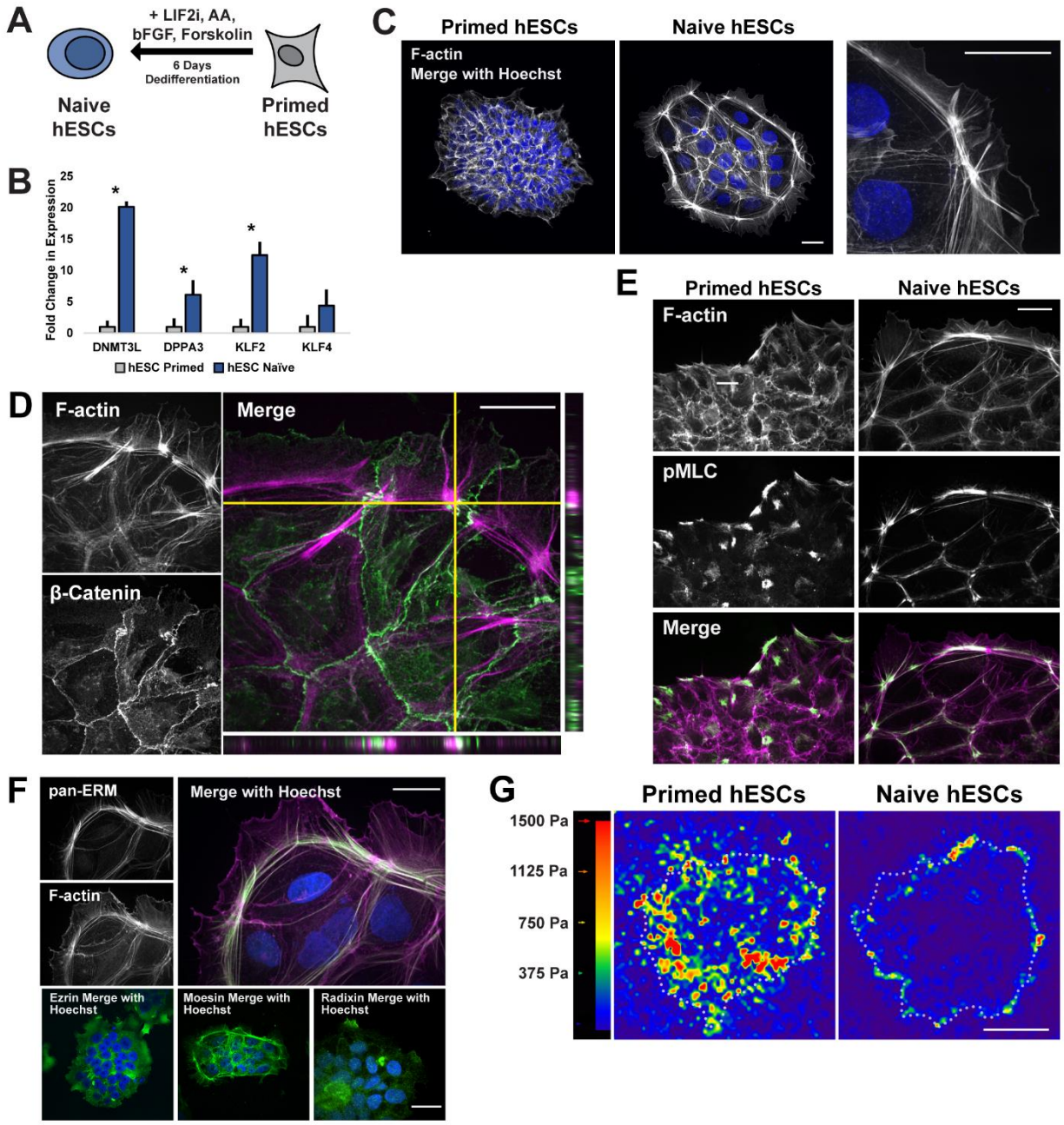

Figure 2.1: Dedifferentiation of primed hESCs to naïve pluripotency includes F-actin filament remodeling and the formation of an actin ring.

Figure 2.1: Dedifferentiation of primed hESCs to naïve pluripotency includes F-actin filament remodeling and the formation of an actin ring.

A, Schematic of the dedifferentiation process from primed to naïve human embryonic stem cells (hESCs). **B**, Confirmation of dedifferentiation indicated by increased expression of pluripotency genes associated with a naïve state as determined by qPCR. Data represent the means ± S.E.M. normalized to Oct4 (n=3 separate cell preparations). *P* values were calculated using a two-tailed Student's *t*-test. **C-G** Images of primed and naïve stem cells stained or immunolabeled for actin cytoskeleton components. **C**, Confocal (left and middle) and super-resolution (right) images of hESCs stained for F-actin with phalloidin (white) and Hoechst (blue) show a bundled actin filament ring encapsulating colonies of naïve but not primed cells. **D-F**, Confocal images of naïve hESCs immunolabeled for β-catenin (**D**), pMLC (**E**), and ERM proteins (**F**) and stained for F-actin with phalloidin (magenta) demonstrating cytoskeletal remodeling. Scale bars, 25 µM. **G**, Representative stress maps generated by traction force microscopy (TFM). Dotted outlines indicate colony borders. Scale bar, 50 µM.

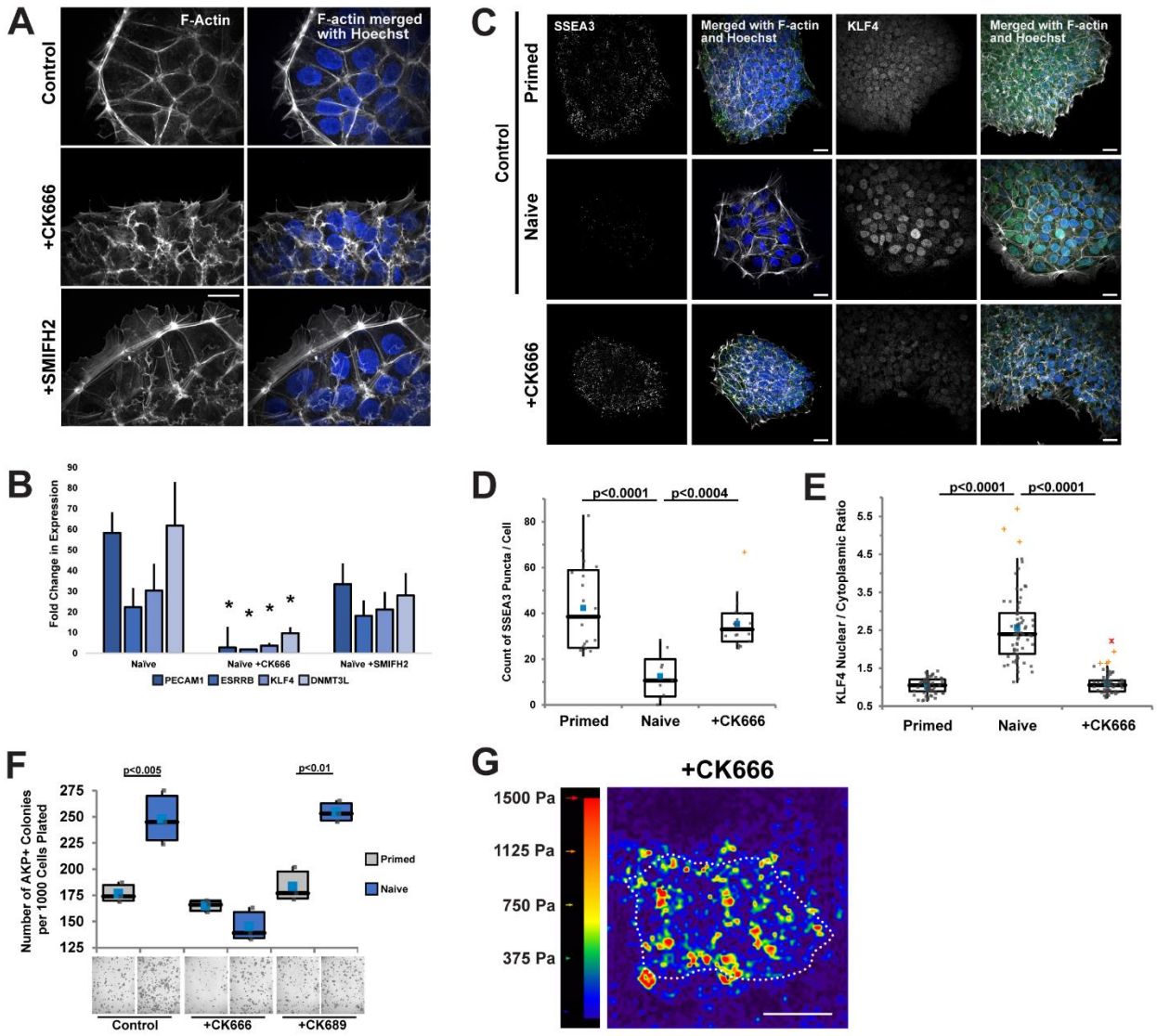

Figure 2.2: Inhibiting Arp2/3 complex but not formin activity blocks formation of an actin ring and dedifferentiation to naïve pluripotency.

Figure 2.2: Inhibiting Arp2/3 complex but not formin activity blocks formation of an actin ring and dedifferentiation to naïve pluripotency.

A, Confocal images of D6 naïve hESCs maintained in the absence (control) or presence of 80 µM CK666 or 50 µM SMIFH2 and stained for F-actin with phalloidin and nuclei with Hoechst. **B**, Expression of the indicated pluripotency transcripts determined by qPCR at D6 of dedifferentiation in the absence (Control) or presence of CK666 or SMIFH2. The Arp2/3-complex activity inhibitor CK666 impairs upregulation of pluripotency genes used to identify naïve pluripotency. Data are the means ± S.E.M. of 3 determinations normalized to Oct4. *P* values were calculated using a two-tailed Student's *t*-test. **C-E**, Confocal images of control primed and naïve hESCs and D6 cells dedifferentiated in the presence of CK666 immunolabeled for the primed marker SSEA3, quantified in (**D**) and the naïve marker KLF4, quantified in (**E**). Box plots in (**D**) and (**E**) show median, first and third quartile, with whiskers extending to observations within 1.5 times the interquartile range. **F**, Clonogenicity, determined by alkaline phosphatase positive colonies (quantified in top panel and representative brightfield images in bottom panel) in control primed and naïve hESC as well as dedifferentiated in the presence of CK666 or 80 µM CK689, an inactive analog of CK666. Data are the means ± S.E.M. normalized to the number of cells plated in 3 separate determinations. Box plots are as described in (**D,E**) with *P* values calculated using a two-tailed Student's *t*-test. Scale bars, 25 µM. **G**, Representative stress maps generated by traction force microscopy (TFM). Dotted outlines indicate colony borders. Scale bar, 50 µM.

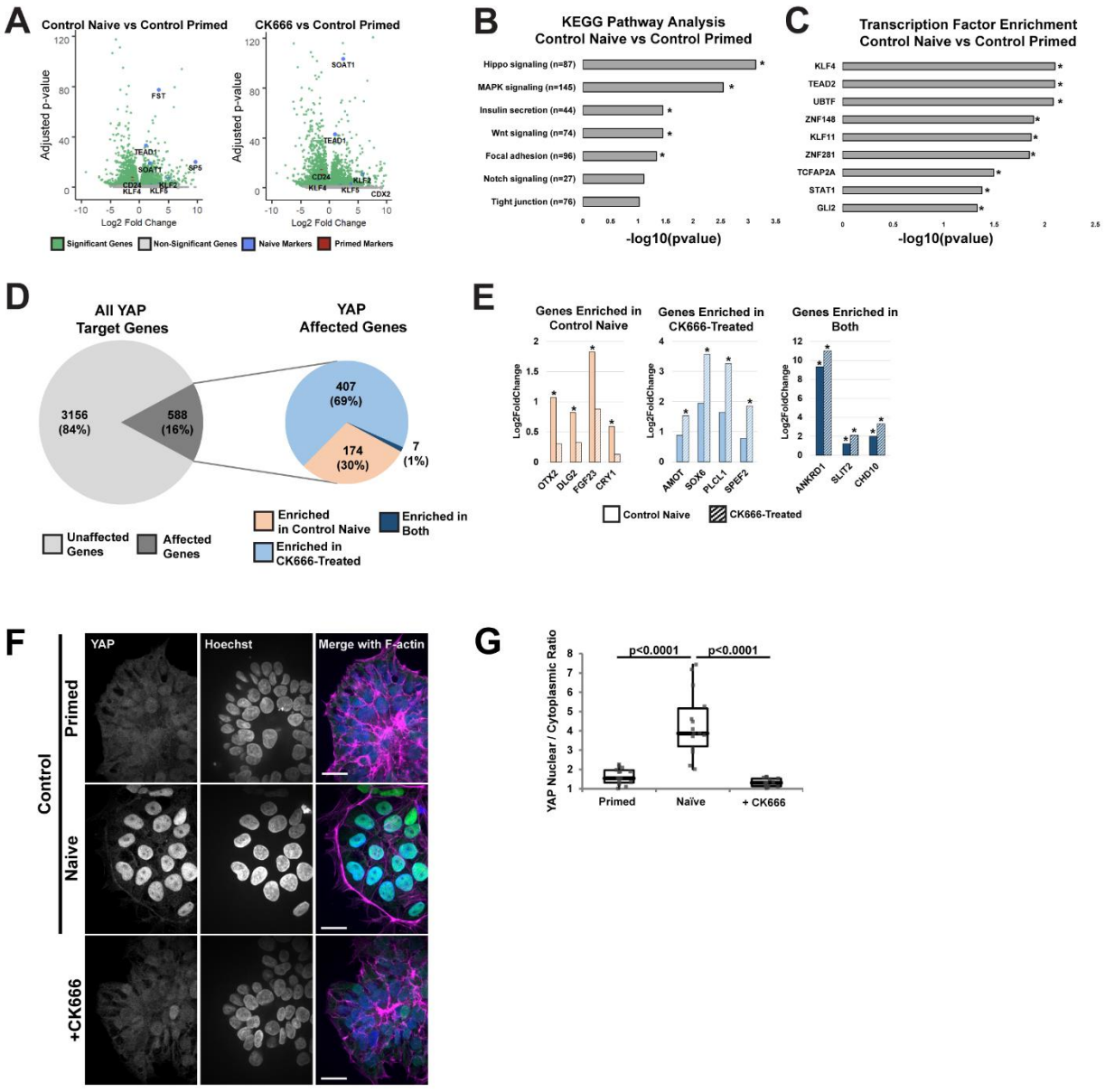

Figure 2.3: Inhibiting Arp2/3 complex activity disrupts Hippo signaling in naïve hESCs.

Figure 2.3: Inhibiting Arp2/3 complex activity disrupts Hippo signaling in naïve hESCs.

A, Volcano plots showing transcriptome fold-changes (*padj*) of dedifferentiations in the absence (Control Naïve) or presence of CK666-treated dedifferentiations compared with primed hESCs. Each dot represents a single gene, with significant genes (padj < 0.05) in green). Notable primed and naïve markers are depicted in red and blue, respectively. **B**,**C** KEGG pathway analysis (**B**) and transcription factor enrichment analysis (**C**) of control primed and naïve hESCs. The number of DEGs indicated in each pathway is displayed and asterisks indicate significantly enriched pathways ($p < 0.05$). **D**, Unbiased screening of all known YAP target genes in dedifferentiated cells in the absence (Control Naive) and presence of CK666. Affected genes were further analyzed to indicate whether they are enriched in control, CK666-treated, or both conditions when compared with primed controls. **E**, Expression of selected YAP target genes from bulk RNAseq, with asterisks indicating significant difference (padj < 0.05). **F**, Representative confocal images of control primed and naïve hESCs and naïve hESCs generated in the presence of 80 µM CK666 immunolabeled for YAP and stained for nuclei with Hoechst and F-actin with phalloidin. **G**, Quantification of nuclear to cytoplasmic ratio of YAP from images as shown in (**F**). Box plots show median, first and third quartile, with whiskers extending to observations within 1.5 times the interquartile range. Data are from 5 separate cell preparations with *P* values calculated using a two-tailed Student's *t*-test. Scale bars, 25 µM.

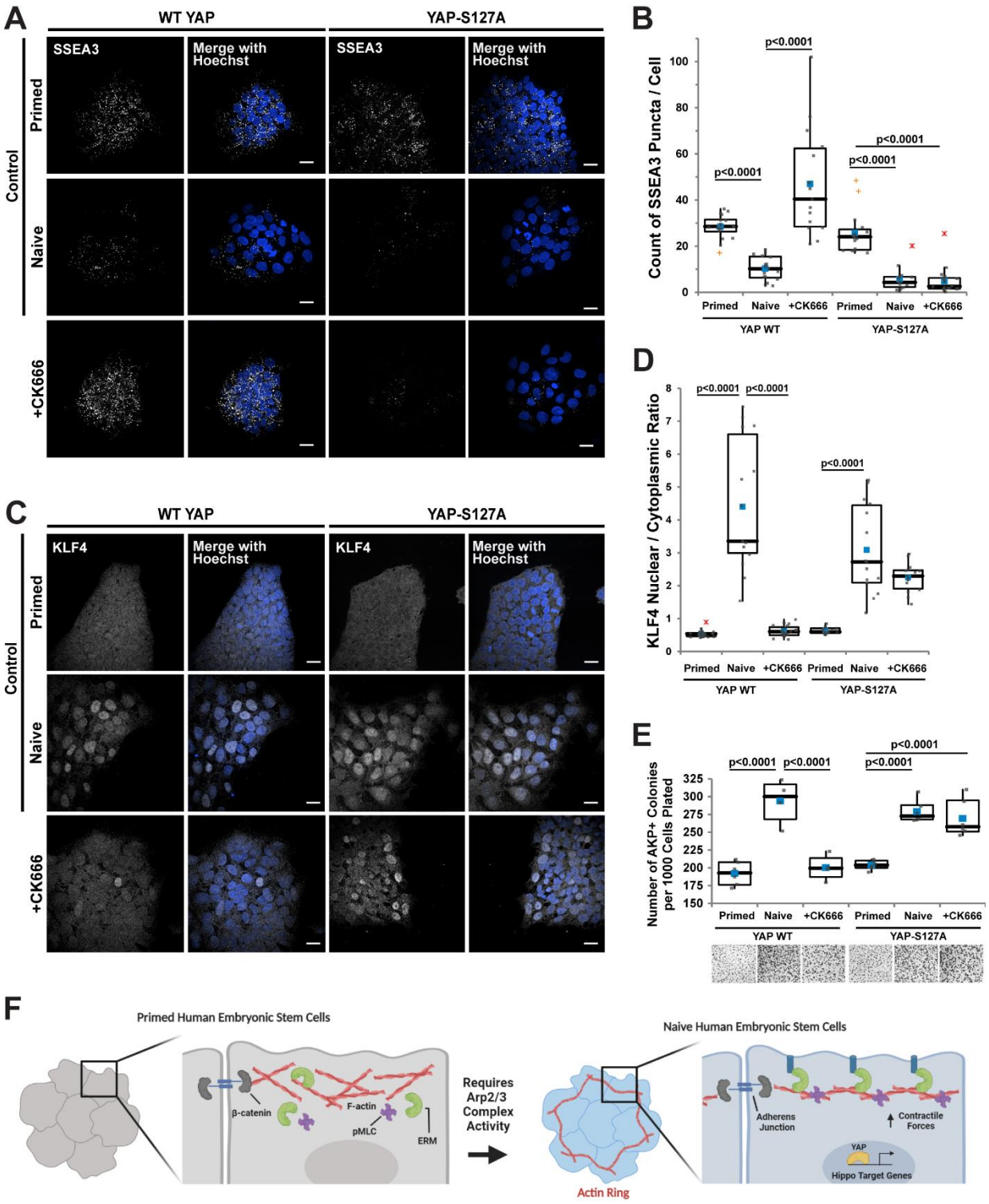

Figure 2.4: Overexpression of YAP-S127A rescues naïve pluripotency blocked with inhibiting Arp2/3 complex activity.

Figure 2.4: Overexpression of YAP-S127A rescues naïve pluripotency blocked with inhibiting Arp2/3 complex activity.

A, C, Representative confocal images of control primed, control naïve cells, and cells dedifferentiated in the presence of CK666 with or without stably overexpressing YAP WT or YAP-S127A immunolabeled for the primed marker SSEA3 (**A**) or the naïve marker KLF4 (**C**) and stained for nuclei with Hoechst and F-actin with phalloidin. **B, D**, Images as in **A** and **C** were used to quantify, respectively, the number of SSEA3 puncta (**B**) and the nuclear to cytoplasmic ratio of KLF4 (**D**). Box are plots as described for Figure 2. **E**, Clonogenicity, determined by alkaline phosphatase positive colonies (quantified in top panel and representative brightfield images in bottom panel) in control primed and naïve hESC, and dedifferentiated in the presence of CK666 with stably expressed YAP WT or YAP-S127A. Data are the means ± S.E.M. normalized to the number of cells plated from 3 separate determinations, with box plots as described for Figure 2 d, e and *P* values are calculated using a two-tailed Student's *t*-test. Scale bars, 25 µM. **F**, Model illustrating cytoskeletal remodeling that occurs during dedifferentiation to a naïve state of pluripotency. Successful dedifferentiation to naïve pluripotency includes the formation of an actin ring structure, uniformity of colony mechanics, recruitment of actin-binding proteins known to play roles in pluripotency, and the regulation of Hippo signaling.

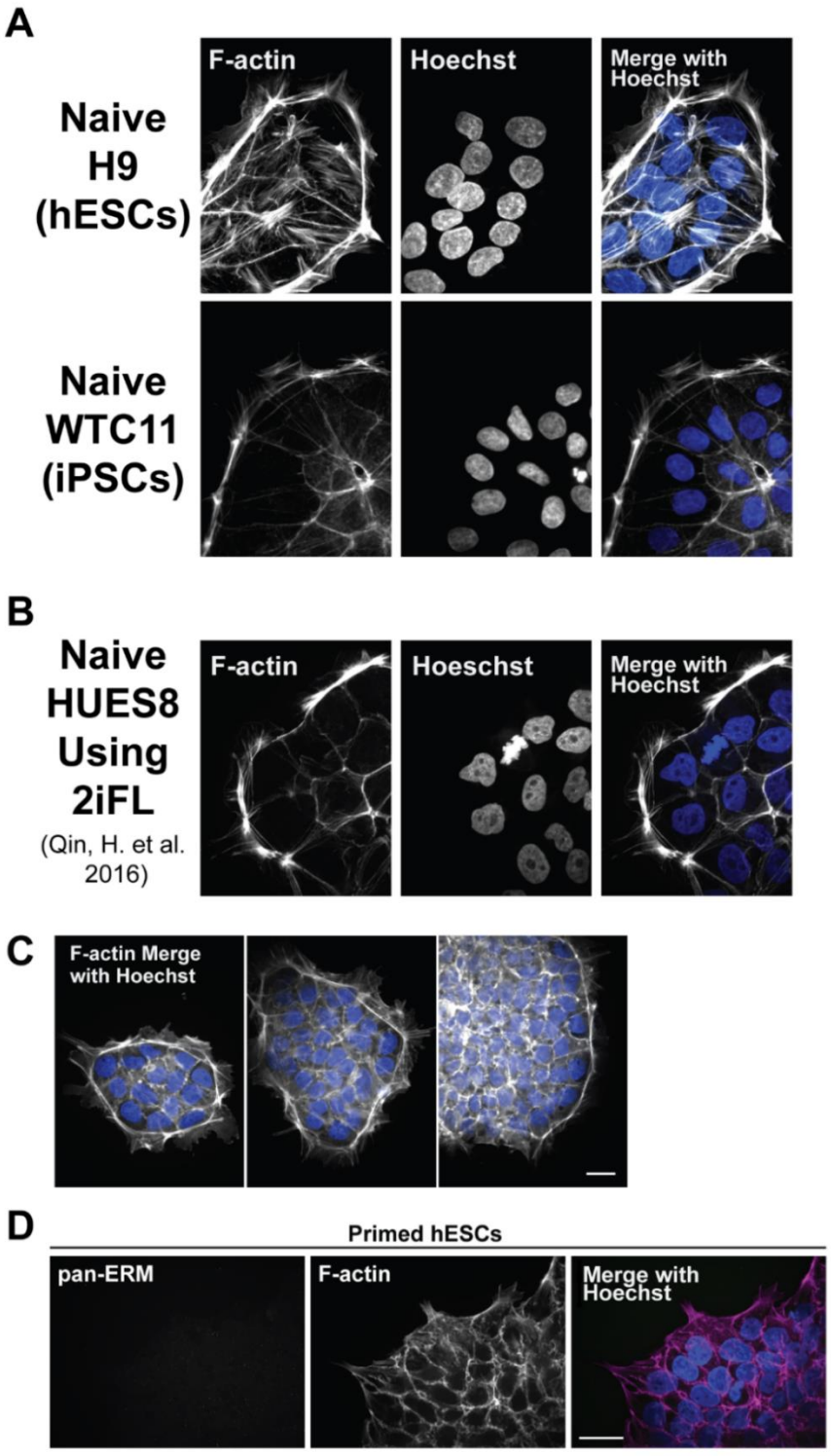

Figure 2.5: Naïve stem cell cytoskeletal remodeling occurs in multiple culture conditions and cell lines.

Figure 2.5: Naïve stem cell cytoskeletal remodeling occurs in multiple culture conditions and cell lines.
A, Confocal images of naïve H9 hESCs and WTC11 iPSCs stained for F-actin with phalloidin. **B**, Confocal images of naïve hESCs using an alternative dedifferentiation medium(Qin et al., 2016). **C**, Confocal images of naïve hESCs at different colony sizes. **D**, Confocal images of primed hESCs immunolabeled with pan-ERM antibodies and stained for F-actin with phalloidin and nuclei with Hoechst. Scale bars, 25 μM.

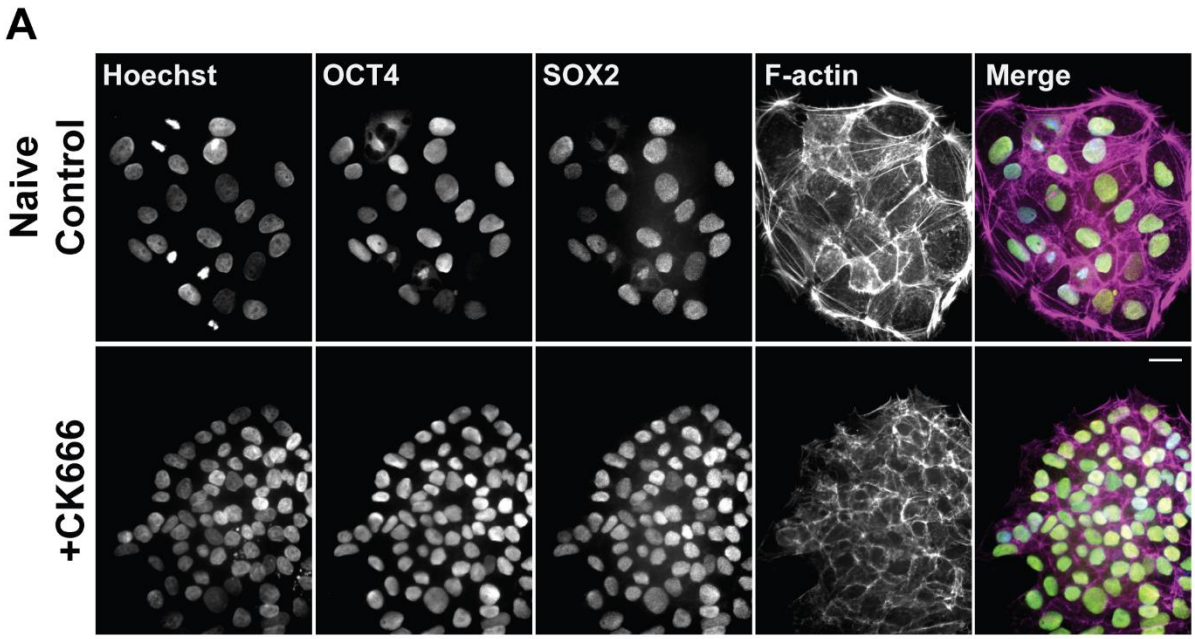

Figure 2.6: Inhibition of Arp2/3 complex activity does not cause an exit from the pluripotent state.
A, Confocal images of naïve hESCs stained for F-actin with phalloidin (magenta) and Hoechst (blue) and immunolabeled for pluripotency markers Oct4 (green) and Sox2 (yellow). Scale bars, 25 µM.

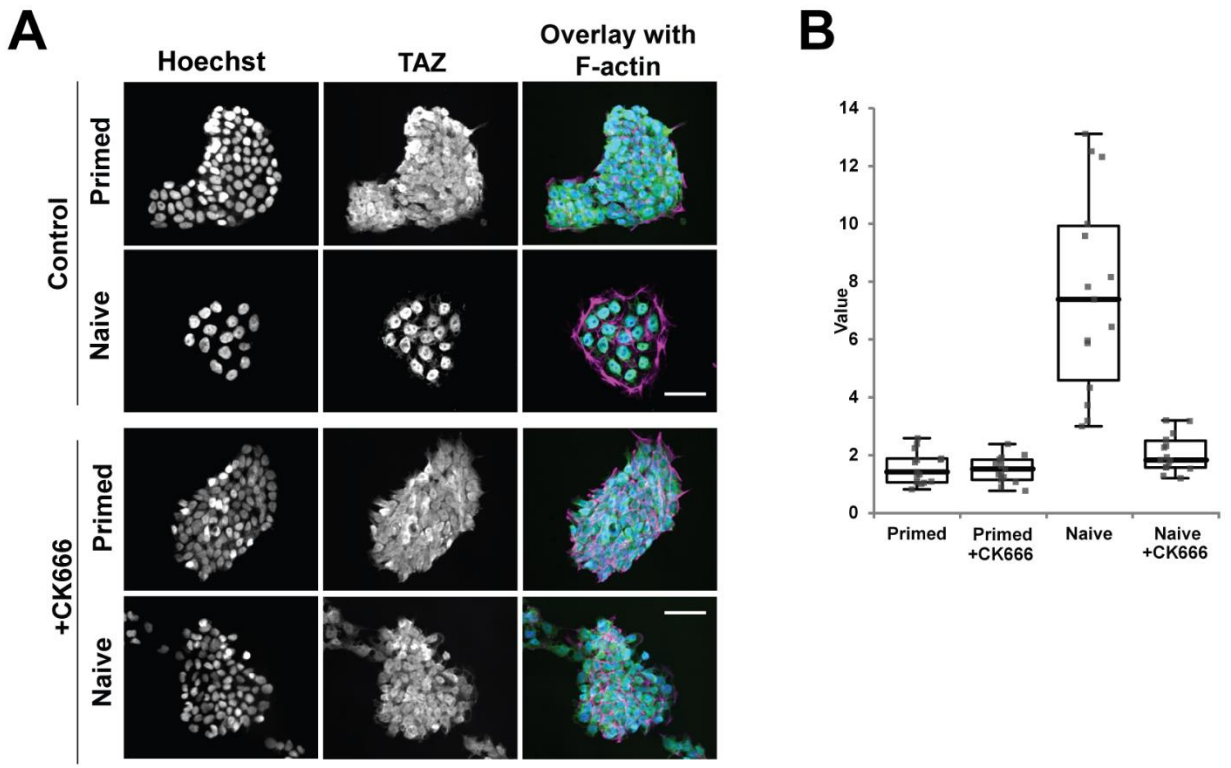

Figure 2.7: The Hippo effector protein TAZ is enriched in the nucleus in naïve stem cells and inhibited with CK666.
A, Confocal images of D6 primed and naïve hESCs in the absence (Control) or presence of 80 µM CK666 immunolabled for TAZ (green) and stained for F-actin with phalloidin (magenta) and Hoechst (blue). **B**, Quantification of nuclear to cytoplasmic ratio of TAZ from images shown in **A**. Box plots show median, first and third quartile, with whiskers extending to observations within 1.5 times the interquartile range. Data are from 5 separate cell preparations with *P* values calculated using a two-tailed Student's *t*-test. Scale bars, 25 µM.

Chapter 3 – Additional Publications from Dissertation Research

3.1 – Preparation of *Drosophila* Ovarioles for Single-Cell RNA Sequencing

The production of eggs in the Drosophila ovary requires complex interactions between multiple cell types that coexist within the same solid tissue. This cellular heterogeneity makes the ovary a rich subject of study, but also makes it challenging to identify transcriptional differences between individual cell types using methods such as bulk RNA sequencing. The development of single-cell RNA sequencing (scRNA-seq) techniques addresses this limitation by providing an avenue to profile genetic and functional heterogeneity at a cellular resolution. Here, we describe the isolation and preparation of the Drosophila ovary for scRNAseq. This protocol emphasizes a short preparation time, high cell viability, prevention of RNA-degradation, and reduction of technical variation to achieve highly reproducible single-cell profiles.

See:

Meyer, N., Peralta, J., Nystul, T. (2023). Preparation of Drosophila Ovarioles for Single-Cell RNA Sequencing. In: Giedt, M.S., Tootle, T.L. (eds) Drosophila Oogenesis. Methods in Molecular Biology, vol 2626. Humana, New York, NY. https://doi.org/10.1007/978-1-0716-2970-3_17

Preparation of Drosophila Ovarioles for Single cell RNA sequencing

Nathaniel Meyer*, Jobelle Peralta*, and Todd Nystul**

*These authors contributed equally to this work

**Corresponding author

Abstract

The production of eggs in the Drosophila ovary requires complex interactions between multiple cell types that coexist within the same solid tissue. This cellular heterogeneity makes the ovary a rich subject of study, but also makes it challenging to identify transcriptional differences between individual cell types using methods such as bulk RNA sequencing. The development of single-cell RNA sequencing (scRNA-seq) techniques addresses this limitation by providing an avenue to profile genetic and functional heterogeneity at a cellular resolution. Here we describe the isolation and preparation of the Drosophila ovary for scRNA-seq. This protocol emphasizes a short preparation time, high cell viability, prevention of RNA-degradation, and reduction of technical variation for the production of highly reproducible single-cell profiles.

Keywords

Single-cell sequencing, Drosophila, ovary

1 – Introduction

Over the past decade, there has been a revolution in the technologies that enable single cell RNA sequencing (scRNA-seq) of whole tissues and organs [1–5]. These exciting developments make it possible to obtain transcriptional profiles of multiple different cell types in a heterogeneous tissue or organ, including rare cell types such as stem and progenitor cells. At the same time, new bioinformatic methods are being developed to analyze the treasure trove of data produced by scRNA-seq experiments. Standard clustering algorithms help to identify transcriptionally distinct subsets of cells that correspond to distinct cell types [6, 7], and other tools build on the output from these algorithms to generate additional predictions, such as the lineage relationships, regulon activity, or cell signaling relationships in specific cell types of interest within the tissue [8–13]. Taken together, these new technologies are providing an unprecedented level of detail about the cellular diversity that exists in complex tissues, as well as the ways in which these cellular populations change over time and in different conditions.

The key innovation that has made scRNA-seq possible is the development of methods to generate a unique cDNA library from each cell in the tissue. The cDNA libraries are generated using primers with a different “barcoding” sequence (or set of sequences) for each cell. This allows the cDNA libraries to be pooled together for sequencing and then sorted back out afterwards by grouping sequences with common barcodes. To generate these cDNA libraries, the tissue is dissociated into a single cell suspension and then each cell is separated into a well or oil droplet where the reactions occur to generate the unique

libraries [1–3]. Alternatively, rather than creating cDNA libraries for each cell separately, the cells can be repeatedly pooled in different combinations so that each cell has a high probability of acquiring a unique set of barcodes [4]. Yet another alternative is to perform RNA sequencing on nuclei isolated from fresh or frozen tissue rather than on whole cells [14]. There are advantages and drawbacks to each approach, so the choice of which one to use depends on several factors, such as the number of cells and depth of sequencing that is desired, the size of the cells, and cost. This protocol was developed to prepare cells from freshly isolated Drosophila ovaries to be submitted for single cell sequencing using the 10x Genomics droplet-based method, which is the method that was used in several recently published single-cell atlases of the Drosophila ovary [15–18]. However, it is likely that this protocol could be adapted for use with other strategies for scRNA-seq of whole cells with very few modifications (*see* **Note 1**).

2 – Materials

Prepare all solutions using molecular grade water (free of RNAses, DNAses, and proteases). Eliminate RNAse contamination from the working area using purifying agents such as RNAseZap or RNAse AWAY. Using freshly prepared reagents is ideal, however aliquoted sterile FBS and solubilized insulin may be prepared beforehand and stored at -20°C. If using frozen reagents, allow at least 1 hour for reagents to thaw on ice prior to use. Preparation of all required buffers and solutions with thawed reagents will take approximately 1 hour. All reagents should be kept on ice or at 4°C until needed. Throughout this protocol, only use LoBind Eppendorf tubes and sterile filter tips.

2.1 Insulin in Acidified Water

1. For 15 mL of Insulin in Acidified Water (1 mg/ mL): Add approximately 10 mL of water to a 15 mL conical tube. Add 15 mg of lyophilized insulin powder. Mix and adjust pH with HCl to pH ~2.5. Allow solution to fully solubilize by gently turning the conical tube for 2 - 3 minutes at room temperature. Solubilize longer if needed. Add molecular grade water to a final volume of 15 mL. Aliquot and store at -20°C (*see* **Note 2**).

2.2 S2 Buffer

1. For 7.2 mL of S2 Buffer: 5.28 mL S2 Medium, 720 µL sterile FBS, 1.2 mL and Insulin (1 mg/mL in acidified water). Sterile filter using a 0.22 µM filter syringe. Keep on ice. (*see* **Note 3**).

2.3 Digestion Buffer

1. For 1 mL of Digestion Buffer: 4 mg/mL of Elastase, 2.5 mg/mL Collagenase, and 1 mL Cell Dissociation Buffer (*see* **Note 4**). Keep on ice or at 4°C until use.

2.4 Resuspension Buffer

1. For 1 mL of resuspension Buffer: 1 mL 1X PBS and 8 µL Ultra-pure BSA (*see* **Note 5**). Keep on ice or at 4°C until use.

3 – Methods

3.1 Preparation of Flies

1. Female flies should be maintained on wet yeast in a bottle or vial for at least 5 days prior to dissections with sufficient males. Feed flies with fresh wet yeast 3-4 hours prior to dissection (*see* **Note 6**).
2. During dissection, moving quickly and efficiently is required. If necessary, sort flies of the desired phenotype the night before dissections. Do not separate females from males prior to dissection. We recommend a ratio of 2 females to 1 male. (*see* **Notes 7 and 8**)

3.2 Ovary Dissection and Enrichment for the Early (Non-Vitellogenic) Stages

1. Isolate 60 pairs of ovaries using standard procedures [19] in S2 Buffer on an ice pack (*see* **Note 9**). Do not separate ovarioles. Complete all dissections, including microdissections within 60 minutes.
2. Transfer isolated ovary pairs into a clean well filled with S2 Buffer (*see* **Note 10**).
3. To enrich for younger, non-vitellogenic stages, grab one ovary pair using forceps then use a scalpel to cut the tissue. Transfer isolated tissue into a clean well filled with S2 Buffer (**Figure 3.1.1).** (*see* **Notes 11 and 12**)
4. Using a pre-wet P200 filter tip, transfer the tissues into a collection tube filled with 200 µL of S2 Buffer on ice (*see* **Note 13**).

3.3 Tissue Digestion and Single Cell Isolation

Before beginning tissue digestion, precool the centrifuge.

1. Wash isolated ovaries with 750 µL of cold, sterile, Cell Dissociation Buffer. Briefly centrifuge tubes (~5 seconds) in a table-top microfuge to pool the tissue. Remove Cell Dissociation Buffer without disturbing the tissue pellet.
2. Add 1 mL of Digestion Buffer to each sample.
3. Continuously pipette the tissue up and down for 20 minutes without introducing air bubbles (*see* **Notes 14 and 15**).
4. Using a pre-wet P200 filter tip, filter samples through a 50 µM filter into a new LoBind Eppendorf tube. Continue to digest the samples by continuously pipetting up and down for another 10 minutes without introducing air bubbles.
5. Using a pre-wet P200 filter tip, filter samples through a 30 µM filter into a new LoBind Eppendorf tube.
6. Quench the digestion by adding 500 µL of S2 Buffer and pellet cells via centrifugation (5 minutes, 4°C, 3500 rcf). Remove the supernatant carefully without disturbing the cell pellet.
7. Gently resuspend and wash cells once with 1 mL of S2 Buffer and pellet cells via centrifugation (5 minutes, 4°C, 3500 rcf). Remove the supernatant carefully without disturbing the cell pellet.
8. Resuspend cells in 200 µL of Resuspension Buffer. Mix well using a P200 to prevent clustering of cells.

3.4 Cell Counting

1. Use a hemocytometer to count dissociated cells (**Figure 3.1.2**). (*see* **Notes 16 and 17**).
    a. Add 10 µL of Trypan Blue to 10 µL of cells from Step 3.3.8. This gives a dilution factor of 2.
    b. Count 4 squares on the hemocytometer. Calculate the cell concentration:
        i. $\frac{Unlabeled\ Cells\ Counted}{Squares\ Counted\ (4)}\ x\ Dilution\ Factor\ (2)\ x\ 10{,}000\ =$

        $Live\ Cells\ per\ mL$

        ii. $\frac{Labeled\ Cells\ Counted}{Squares\ Counted\ (4)}\ x\ Dilution\ Factor\ (2)\ x\ 10{,}000\ =$

        $Dead\ Cells\ per\ mL$
    c. Calculate the total cell number:
        i. $\frac{Live\ Cells\ per\ mL}{1000\ \mu L\ /\ mL}\ x\ Volume\ Remaining\ (e.g.\ 190\ \mu L)\ =$

        $Total\ Live\ Cells$
    d. Dilute cells with Resuspension Buffer to a final concentration required by the single cell genomics platform you are using (*see* **Note 17**).

The sample is now ready to be submitted for single cell sequencing using a method such as the 10x Genomics platform.

4 – Notes

1. The germ cells and many of the follicle cell types in late-stage follicles are too big to be captured by the oil droplets in the 10x Genomics method, so these stages are removed in this protocol (see Section 3.2, step 3). However, other methods, such as those in which cells are sorted into individual wells of a multiwell plate, may be able to capture the larger cell types in the ovary. When using these methods, it may be desirable to skip Step 3 of Section 3.2 and retain the later stages.
2. Insulin has low solubility at neutral pH. Solubilize using hydrochloric acid in water at pH 2-3. Stock solutions can be prepared, aliquoted, and stored at -20°C in single-use aliquots. Avoid freeze-thaw cycles.
3. The S2 Buffer is used both during the dissection as well as collection of each tissue sample. We found that approximately 7 mL of S2 Buffer per sample is sufficient to thoroughly wash and clean each tissue sample with minimal waste.
4. 1 mL of Digestion Buffer per sample is required. It is important that the elastase and collagenase are fresh. Using expired enzymes in this step will reduce yield of single cells as well as decrease viability.
5. 200 µL of Resuspension Buffer per sample is required. The addition of BSA helps prevent cells from clumping together or sticking to any tips or tubes. Make no less than 1 mL of Resuspension Buffer at once.
6. Feeding flies with wet yeast causes the ovary to be healthy and plump up. By feeding with wet yeast for at least 5 days prior to dissection, we ensure the tissue

is healthy. In addition, feeding the flies with fresh wet yeast 3-4 hours prior to dissection helps enlarge the ovary, which makes the ovary isolation and microdissection steps easier.

7. In some cases, it may be time consuming to identify the flies of the correct genotype. In these cases, it may be beneficial to isolate a large number of flies with the required genotype before starting the dissection process.
8. The number of ovary pairs dissected can be changed. In cases where flies with the genotype of interest was relatively rare, we have used as little as 15 ovary pairs and found that we were still able to recover enough cells. However, we recommend aiming for approximately 60 pairs of ovaries if possible to ensure that a sufficient number of cells remain at the end of the protocol.
9. We recommend completing the tissue dissection and beginning digestion within 60 minutes. We found no noticeable difference in the amount of cell death during shorter dissection times. However, exceeding this time yielded noticeably larger amounts of dead cells in the final cell count. If cells from multiple different populations of flies (e.g. different genotypes or experimental conditions) will be submitted at the same time, we recommend organizing a “dissection party” in which each population of flies is assigned to a different person and the ovary dissections occur in parallel. This will help ensure that the process is completed within this timeframe and at the same time for all samples.
10. Moving the tissue through serial washes of S2 Buffer during the dissection helps clean the tissue. We found it easier to complete the dissection in 2-3 sets of 20-30

ovary pairs. Preparing 2-3 sets of dissection wells with S2 Buffer also prevented the dissection wells from accumulating debris from the dissections.

11. The microdissection of the ovary to isolate the early stages can be difficult to perform in a quick, reproducible manner. The goal is to be able to isolate 60 pairs of ovaries, microdissect away the later stages, and pool the tissue together in a collection tube within 60 minutes. We recommend practicing these dissections prior to performing the full experiment.
12. We do not recommend using scissors for this process. We found scissors to be difficult to position carefully, leading to poor enrichment of the earlier stages in the final isolate. In comparison, a scalpel can be positioned much more precisely.
13. Throughout this protocol, we recommend pre-wetting all pipette tips. The isolated tissue can easily stick to the sides of the pipette tip. Pre-wetting the pipette tips minimizes tissue loss.
14. Set a P200 to ~175 µL to prevent material contacting the filter while pipetting the tissue. During this process, the solution will become turbid, this is normal and expected.
15. If digesting more than one sample, place tubes on a nutator when not pipetting. We recommend that one person work on no more than two samples, pipetting each sample for 1 - 2 minutes before switching samples. If a single person processes more than 2 samples, the tissue may not be fully digested within the recommend time.

16. When preparing single cell suspensions from 60 ovary pairs, we commonly achieved a yield of approximately 2-3 X 10^6 live cells and a viability ≥85%.
17. Use a hemocytometer and count manually rather than using an automated cell counter. In our experience, automated cell counters are not calibrated for the size of Drosophila ovarian cells, and thus give inaccurate cell counts. We also found that assessing the single-cell suspension manually allowed us to determine if the single-cell prep was performed well (see **Figure 3.1.2**)
18. We recommend preparing excess sample for submission and keeping the single cell isolation on ice until the sample is submitted. For example, our core facility requested that we provide 20,000 cells per sample, so we submitted 30,000 cells in 30 µL of Resuspension Buffer (a final concentration of 1,000 cells per µL).

Figures

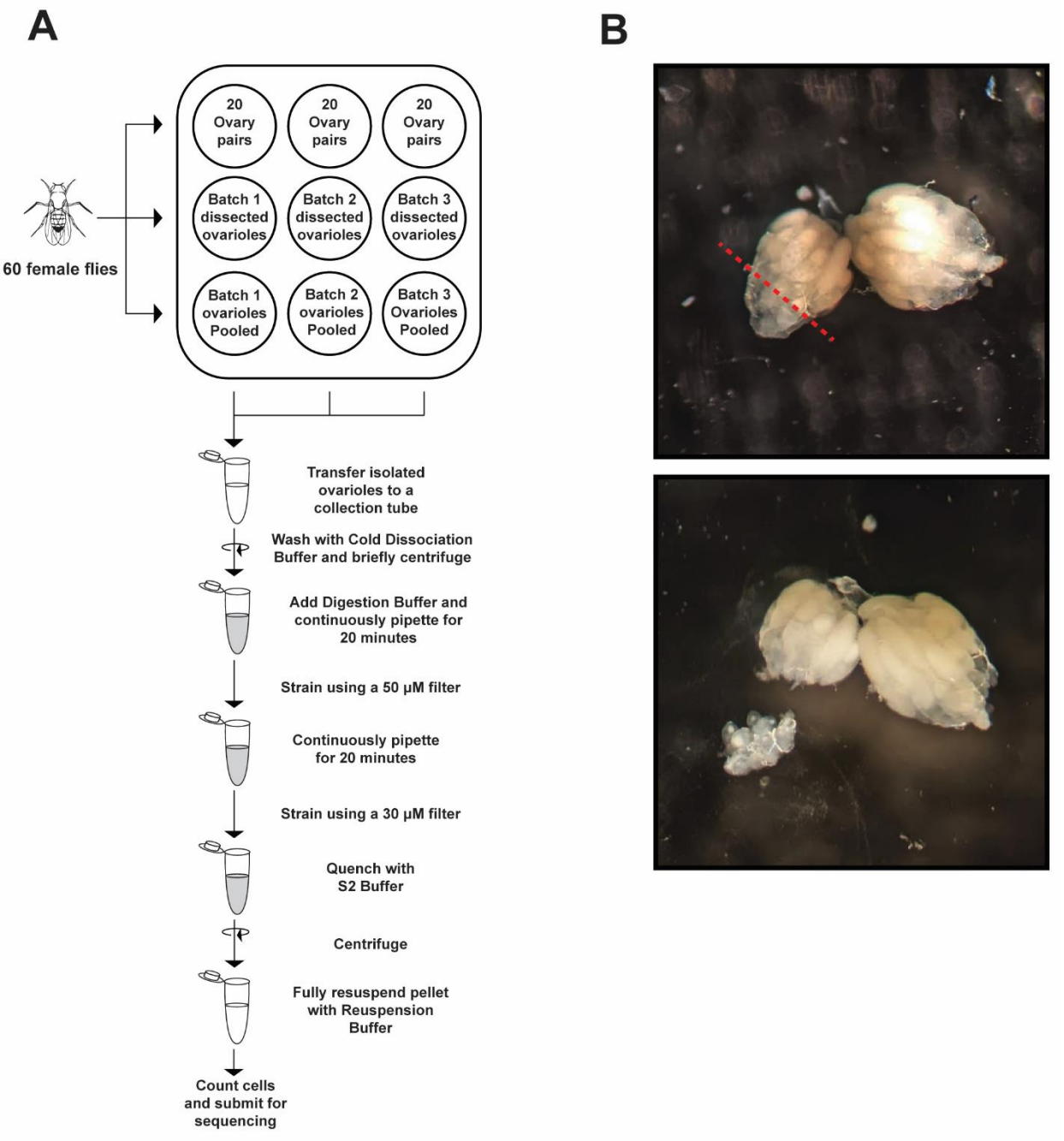

Figure 3.1.1: Ovary dissection and enrichment for the early (non-vitellogenic) stages.

Figure 3.1.1: Ovary dissection and enrichment for the early (non-vitellogenic) stages.

Microdissection strategy for the isolation of non-vitellogenic stages of Drosophila ovaries. (A) Under a dissecting microscope, the non-vitellogenic stages of the ovarioles within the ovary can be identified by their transparent morphology. Cutting along the border of the transparent non-vitellogenic stages and opaque vitellogenic stages enriches for the region of the earlier stages of oogenesis. (B) After cutting the tissue, the non-vitellogenic stages should remain attached as long as the ovarioles were not separated. This makes it easier to put the tissue into a tube.

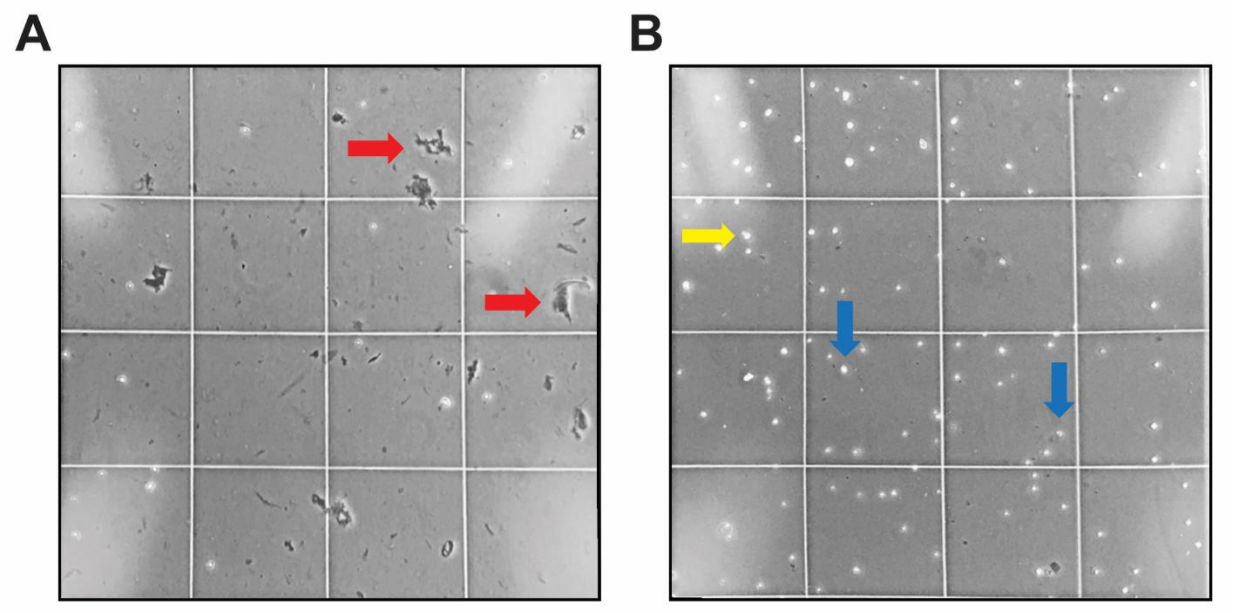

Figure 3.1.2: Counting cells in a single cell suspension.

Representative single cell isolates from Drosophila ovarian tissue, enriched for the early stages of oogenesis. It is important to assess the quality of the single cell isolate prior to submission for sequencing. (A) In a poor isolation, debris was present (red arrows) and there were not enough cells to meet the requirements for submission. (B) In a high-quality isolation, less debris was observed, the overall number of cells that are fully dissociated (i.e. not in doublets or higher order clusters, blue arrows) was high, and the number of dead cells was low.

Acknowledgements

This protocol is based on a protocol that was originally developed in our lab by Dr. Katja Rust, with input from Dr. Maija Slaidina. We are grateful to them for their contributions.

References

1. Zheng GXY, Terry JM, Belgrader P, et al (2017) Massively parallel digital transcriptional profiling of single cells. Nat Commun 8:14049
2. Macosko EZ, Basu A, Satija R, et al (2015) Highly Parallel Genome-wide Expression Profiling of Individual Cells Using Nanoliter Droplets. Cell 161:1202–1214
3. Klein AM, Mazutis L, Akartuna I, et al (2015) Droplet barcoding for single-cell transcriptomics applied to embryonic stem cells. Cell 161:1187–1201
4. Rosenberg AB, Roco CM, Muscat RA, et al (2018) Single-cell profiling of the developing mouse brain and spinal cord with split-pool barcoding. Science 360:176–182
5. Hwang B, Lee JH, Bang D (2018) Single-cell RNA sequencing technologies and bioinformatics pipelines. Exp Mol Med 50:1–14
6. Satija R, Farrell JA, Gennert D, et al (2015) Spatial reconstruction of single-cell gene expression data. Nat Biotechnol 33:495–502
7. Kiselev VY, Andrews TS, Hemberg M (2019) Challenges in unsupervised clustering of single-cell RNA-seq data. Nat Rev Genet 20:273–282
8. Qiu X, Mao Q, Tang Y, et al (2017) Reversed graph embedding resolves complex single-cell trajectories. Nat Methods 14:979–982
9. Aibar S, González-Blas CB, Moerman T, et al (2017) SCENIC: single-cell regulatory network inference and clustering. Nat Methods 14:1083–1086
10. La Manno G, Soldatov R, Hochgerner H, et al (2017) RNA velocity in single cells. bioRxiv 206052

11. Efremova M, Vento-Tormo M, Teichmann SA, Vento-Tormo R (2020) CellPhoneDB: inferring cell-cell communication from combined expression of multi-subunit ligand-receptor complexes. Nat Protoc 15:1484–1506
12. Browaeys R, Saelens W, Saeys Y (2020) NicheNet: modeling intercellular communication by linking ligands to target genes. Nat Methods 17:159–162
13. Jin S, Guerrero-Juarez CF, Zhang L, et al (2021) Inference and analysis of cell-cell communication using CellChat. Nat Commun 12:1088
14. McLaughlin CN, Brbić M, Xie Q, et al (2021) Single-cell transcriptomes of developing and adult olfactory receptor neurons in Drosophila. Elife 10:. https://doi.org/10.7554/eLife.63856
15. Li H, Janssens J, De Waegeneer M, et al (2021) Fly Cell Atlas: a single-cell transcriptomic atlas of the adult fruit fly. bioRxiv 2021.07.04.451050
16. Rust K, Byrnes LE, Yu KS, et al (2020) A single-cell atlas and lineage analysis of the adult Drosophila ovary. Nat Commun 11:5628
17. Jevitt A, Chatterjee D, Xie G, et al (2020) A single-cell atlas of adult Drosophila ovary identifies transcriptional programs and somatic cell lineage regulating oogenesis. PLoS Biol 18:e3000538
18. Slaidina M, Gupta S, Banisch TU, Lehmann R (2021) A single-cell atlas reveals unanticipated cell type complexity in Drosophila ovaries. Genome Res 31:1938–1951
19. Wong LC, Schedl P (2006) Dissection of Drosophila ovaries. J Vis Exp 52

3.2 – Lineage dynamics of murine pancreatic development at single-cell resolution

Organogenesis requires the complex interactions of multiple cell lineages that coordinate their expansion, differentiation, and maturation over time. Here, we profile the cell types within the epithelial and mesenchymal compartments of the murine pancreas across developmental time using a combination of single-cell RNA sequencing, immunofluorescence, in situ hybridization, and genetic lineage tracing. We identify previously underappreciated cellular heterogeneity of the developing mesenchyme and reconstruct potential lineage relationships among the pancreatic mesothelium and mesenchymal cell types. Within the epithelium, we find a previously undescribed endocrine progenitor population, as well as an analogous population in both human fetal tissue and human embryonic stem cells differentiating toward a pancreatic beta cell fate. Further, we identify candidate transcriptional regulators along the differentiation trajectory of this population toward the alpha or beta cell lineages. This work establishes a roadmap of pancreatic development and demonstrates the broad utility of this approach for understanding lineage dynamics in developing organs.

See:

Byrnes, L.E., Wong, D.M., Subramaniam, M., **Meyer, N.P**., et al. Lineage dynamics of murine pancreatic development at single-cell resolution. Nat Commun 9, 3922 (2018). https://doi.org/10.1038/s41467-018-06176-3

nature COMMUNICATIONS

ARTICLE

DOI: 10.1038/s41467-018-06176-3 OPEN

Lineage dynamics of murine pancreatic development at single-cell resolution

Lauren E. Byrnes[1], Daniel M. Wong[1], Meena Subramaniam[2], Nathaniel P. Meyer[1], Caroline L. Gilchrist[1], Sarah M. Knox[3], Aaron D. Tward[4], Chun J. Ye[2] & Julie B. Sneddon[1]

Organogenesis requires the complex interactions of multiple cell lineages that coordinate their expansion, differentiation, and maturation over time. Here, we profile the cell types within the epithelial and mesenchymal compartments of the murine pancreas across developmental time using a combination of single-cell RNA sequencing, immunofluorescence, in situ hybridization, and genetic lineage tracing. We identify previously underappreciated cellular heterogeneity of the developing mesenchyme and reconstruct potential lineage relationships among the pancreatic mesothelium and mesenchymal cell types. Within the epithelium, we find a previously undescribed endocrine progenitor population, as well as an analogous population in both human fetal tissue and human embryonic stem cells differentiating toward a pancreatic beta cell fate. Further, we identify candidate transcriptional regulators along the differentiation trajectory of this population toward the alpha or beta cell lineages. This work establishes a roadmap of pancreatic development and demonstrates the broad utility of this approach for understanding lineage dynamics in developing organs.

[1] Diabetes Center, University of California, San Francisco, 513 Parnassus Avenue, San Francisco, CA 94143, USA. [2] Institute for Human Genetics, University of California, San Francisco, 513 Parnassus Avenue, San Francisco, CA 94143, USA. [3] Department of Cell and Tissue Biology, University of California, San Francisco513 Parnassus Avenue CA 94143, USA. [4] Department of Otolaryngology-Head and Neck Surgery, University of California, San Francisco 513 Parnassus Avenue CA 94143, USA. These authors contributed equally: Lauren E. Byrnes, Daniel M. Wong. Correspondence and requests for materials should be addressed to J.B.S. (email: julie.sneddon@ucsf.edu)

Figure 3.2: Lineage dynamics of murine pancreatic development at single-cell resolution.

Chapter 4 – Methods

Cell Culture

Primed human embryonic stem cell lines HUES8, H9, and WTC11 were maintained on Matrigel (Corning Life Science #354277) in feeder-free mTeSR-1 medium (STEMCELL Technologies # 85850) at 37°C with 5% CO_2 with daily medium changes. Cells were passaged approximately every 3 days, by dissociating with Accutase (STEMCELL Technologies #07920) and including the Rho-associated coiled-coil kinase (ROCKi) inhibitor Y-276932 (10 μM; Selleckchem #S1049) in the plating medium to facilitate survival. All cell lines were routinely confirmed to be negative for mycoplasma by testing with a MycoAlert Mycoplasma Detection Kit (Lonza # LT07-701).

Generation of Naïve hESCs

Dedifferentiation was completed using previously published methods (Duggal et al., 2015; Qin et al., 2016). Cells were plated at a density of 10,000 cells per cm^2 in the presence of ROCKi (10μM). After 24 h, cells were washed 3 times with PBS and incubated in naïve dedifferentiation medium of mTeSR-1 supplemented with 12 ng/mL bFGF (Peprotech #AF-100-18B), 1 μM PD0325901 (MEKi, Selleckchem #S1036), 3 μM CHIR99021 (GSK3βi, Selleckchem # S2924), 10 μM Forskolin (StemCell Technologies #72112), 50 ng/mL ascorbic acid (Sigma # A92902), and 1000 U recombinant human LIF (StemCell Technologies #78055). Medium was replaced daily, and cells were passaged every 3 days with Accutase. Where indicated, the naïve dedifferentiation medium 2iFL was used, which was mTeSR-1 supplemented with 0.5 μM PD0325901, 3 μM CHIR9902, 10 μM Forskolin, and 1000 U recombinant human LIF. For actin nucleator experiments, naïve

dedifferentiation media was supplemented with either 80 μM CK666 (EMD Millipore #182515), 80 μM CK689 (EMD Millipore #182517), or 50 μM SMIFH2 (Sigma #S4826).

qPCR

Total RNA was isolated using RNAeasy Mini Plus (Qiagen #74134) kits and cDNA was generated using iScript cDNA Synthesis kits (Bio-Rad #1708890) as per the manufacturers specifications. Quantitative PCR was performed using iQ SYBR Green Supermix (Bio-Rad #1708882) and analyzed on a QuantStudio six Flex Real-Time PCR System (Applied Biosystems). For qPCR primer sequences, see **Table 4.1**.

Staining and Immunolabeling

For microscopy, cells were plated on Matrigel-coated glass coverslips prepared using an ultrasonic cleaning bath (Branson). In brief, coverslips were sonicated for 20 minutes in the presence of diluted Versa-Clear (FisherScientific #18-200-700) in double distilled H_2O (ddH_2O), washed three times using ddH_2O, sonicated for 20 minutes in ddH_2O, washed three times using ddH_2O, and were sterilized and stored in 70% ethanol. Cells were maintained for indicated times, typically 3 days, washed briefly with PBS, fixed with 4% PFA for 12 minutes at room temperature, permeabilized with 0.1% Triton X-100 in PBS for 5 minutes, and incubated with blocking buffer consisting of 0.1% Triton X-100 in PBS and 1% BSA for 1 h. Cells were then incubated with primary antibodies diluted in blocking buffer overnight at 4°C, washed with PBS three times, and incubated for 1 hour at room temperature with secondary antibodies, followed by a final PBS 3X wash, with the second

wash containing Hoechst 33342 (1:10,000; Molecular Probes #H-3570) to stain nuclei. To stain for actin filaments, either rhodamine phalloidin (1:400, Invitrogen # R415) or Phalloidin-iFluor 647 (1:1000, Abcam # ab176759) was added to the secondary antibody incubation. For antibody information, see **Table 4.2**.

Confocal and Superresolution Image Acquisition and Quantification

Cells were imaged using an inverted microscope system (Nikon Eclipse TE2000 Perfect Focus System; Nikon Instruments) equipped with a spinning-disk confocal scanner unit (CSU10; Yokogawa), a 488-nm solid-state laser (LMM5; Spectral Applied Research), and a multipoint stage (MS-2000; Applied Scientific Instruments). A CoolSnap HQ2 cooled charge-coupled camera (Photometrics) was used to take images with a camera triggered electronic shutter controlled by NIS Elements Imaging Software (Nikon) and a 60X Plan Apochromat TIRF 1.45 NA oil immersion objective. High resolution and superresolution images were acquired using a Yokogawa CSU-W1/SoRa spinning disk confocal system (Yokogawa) and an ORCA Fusion BT sCMOS camera (Hamamatsu) using 2x2 camera binning. Nuclear-to-cytoplasmic ratios of immunolabeled proteins and number of puncta per cell were quantified using NIS Elements Imaging Software (Nikon). Briefly, the fluorescence in the nucleus (detected by Hoescht) and in the cytoplasm were manually sampled by selection of regions-of-interest. Three regions-of-interest outside of any cell were used to calculate background fluorescence and was subtracted from both nuclear and cytoplasmic fluorescence values. The ratio of fluorescence was then determined by diving the nuclear fluorescence intensity with that of the cytoplasm for a given cell.

Quantification of puncta for SSEA3 was done by creating a 3D projection of full-cell z-stacks by using NIS Elements Imaging Software. Surfaces were created using the 3D thresholding tool normalized across all images and the total number of puncta was recorded. The total number of cells was then counted, as determined by the number of Hoescht positive nuclei, and the number of puncta per cell was calculated by dividing the total number of puncta by the number of cells in each field of view.

Colony Formation Assay

To determine clonogenic potential, cells were dissociated with Accutase and plated on Matrigel-coated 6-well dishes at a density of 1,000 cells per cm^2 in the presence of ROCKi (10 μM). Five days after plating, cells were stained for alkaline phosphatase as per the manufacturer's protocol (StemAb Alkaline Phosphatase Staining Kit II, ReproCell #00-0055) and imaged using a Leica DFC 7000t microscope. To quantify the number of alkaline phosphatase positive colonies, images were analyzed using Fiji (Schindelin et al., 2012).

Library Preparation and RNA Sequencing

RNA was extracted using RNeasy Mini kits (Qiagen) according to the manufacturer's instructions and concentrations were determined by NanoDrop. Library preparation and RNA sequencing were performed by Novogene Co. Ltd (USA). Briefly, RNA purity was measured using a NanoPhotometer spectrophotometer (IMPLEN). RNA integrity and quantity were determined using a Bioanalyzer 2100 system (Agilent Technologies). Three

paired biological replicate libraries were prepared for each condition, with each library generated with 1 µg of RNA per sample. Sequencing libraries were generated using NEBNext Ultra RNA Library Prep Kit for Illumina (NEB) following manufacturer's recommendations and index codes were added to attribute sequences to each sample. Briefly, mRNA was purified from total RNA using poly-T oligo-attached magnetic beads. Fragmentation was carried out using divalent cations under elevated temperature in NEBNext First Strand Synthesis Reaction Buffer (5X). First strand cDNA was synthesized using random hexamer primer and M-MuLV Reverse Transcriptase (RNase H-). Second strand cDNA synthesis was subsequently performed using DNA Polymerase I and RNase H. Remaining overhangs were converted into blunt ends via exonuclease/polymerase activities. After adenylation of 3' ends of DNA fragments, NEBNext Adaptor with hairpin loop structure were ligated to prepare for hybridization. In order to select cDNA fragments of preferentially 150~200 bp in length, the library fragments were purified with AMPure XP system (Beckman Coulter, Beverly, USA). Then 3 µl USER Enzyme (NEB, USA) was used with size-selected, adaptorligated cDNA at 37 °C for 15 min followed by 5 min at 95°C before PCR. Then PCR was performed with Phusion High-Fidelity DNA polymerase, Universal PCR primers and Index (X) Primer. At last, PCR products were purified (AMPure XP system) and library quality was assessed on the Agilent Bioanalyzer 2100 system.

RNA Sequencing Analysis

Raw data (raw reads) were processed through fastp to remove adapters, poly-N sequences, and reads with low quality. Q20, Q30 and GC content of the clean data were calculated and found to be within the normal range. All the downstream analyses were based on the clean data with high quality. Reference genome (ID: 51) and gene model annotation files were downloaded from genome website browser (NCBI) directly. Paired-end clean reads were aligned to the reference genome using the Spliced Transcripts Alignment to a Reference (STAR) software. FeatureCounts was used to count the read numbers mapped of each gene. And then RPKM of each gene was calculated based on the length of the gene and reads count mapped to this gene. Differential expression analysis was performed using DESeq2 R package. The resulting P values were adjusted using the Benjamini and Hochberg's approach for controlling the False Discovery Rate (FDR). Genes with a padj < 0.05 found by DESeq2 were assigned as differentially expressed. The R package clusterProfiler was used to test the statistical enrichment of differential expression genes in KEGG pathways. KEGG terms with padj < 0.05 were considered significant enrichment. Transcription factor binding motif analysis was performed using Enrichr(E. Y. Chen et al., 2013; Kuleshov et al., 2016). To investigate YAP target gene expression, supplementary tables generated as previously described (Pagliari et al., 2020 and Estarás et al. 2017, see Supplemental Methods) were used to generate YAP target gene lists (Estarás et al., 2017; Pagliari et al., 2021).

Plasmids, Site-Directed Mutagenesis, and Generation of Lentivirus

pGAMA-YAP was a gift from Miguel Ramalho-Santos (Addgene plasmid #74942). Site-directed mutagenesis was performed on the pGAMA-YAP construct to create p-GAMA-YAP-S127A using the QuikChange Lightning kit (Agilent Technologies #210513). Forward primers used for the Ser-to-Ala substitution was as follows: 5′-GTTCGAGCTCATGCCTCTCCAGC-3′ and 5’-GCTGGAGAGGCATGAGCTCGAAC-3’. The pGAMA-YAP-S127A plasmid was confirmed via DNA sequencing. To prepare lentivirus, HEK293-FT (Invitrogen # R70007) cells were grown in Dulbecco’s Modified Eagle Medium (ThermoFisher #11965118) supplemented with 10% fetal bovine serum (Peak Serum #PS-FB4), non-essential amino acids (UCSF CCF #CCFGA001), pen/strep (UCSF CCF #CCFGK003), and sodium pyruvate (UCSF CCF #CCFGE001) and maintained at 37°C with 5% CO_2. Lentivirus was generated according to the manufacturer’s specifications by co-transfecting HEK293-FT’s with a mixture of packaging plasmids (ViraPower Lentivirus Expression System; ThermoFisher #K497500). Briefly, 5 x 10^6 HEK293-FT’s were seeded onto a 10 cm dish containing 10 mL of complete medium without antibiotics. After 24h, cells were transfected with a mixture of 3 µg of the lentiviral plasmid containing the gene of interest and 9 µg of the ViraPower Packaging Mix using Lipofectamine™ 2000 (ThermoFisher # 11668030). At 72 hours post-transfection, supernatant was collected, filtered, and concentrated using Lenti-X Concentrator (Takarabio #631231). Concentrated viral supernatant was aliquoted and stored at -80°C.

To generate hESC lines stably expressing WT-YAP and YAP-S127A, primed HUES8 cells were grown to approximately 60% confluency in one well of a 6-well plate. Medium was aspirated, washed once with PBS, and cells were then fed with 1mL fresh media containing 2 µg of polybrene (Millipore Sigma #TR-1003-G), and incubated for 15 minutes at 37°C. Concentrated virus supernatant (100 µL) was added and after 6-8 hours 1 mL of fresh medium was added. After 36 h, viral particles were removed by replacing medium. Three days after virus infection, hESCs were passaged and expanded to three wells in a 6 well-plate. After reaching ~75% confluency, cells were sorted for high mCherry expression by using a BD FACS Aria3u, with sorted cell maintain with 1X penicillin/streptomycin for 3 days and then maintained in standard antibiotic-free TESR+ media.

Tables

Table 4.1: List of qPCR Primers

qPCR Primer Name	Sequence (5’ to 3’)
GAPDH_for	ACAACTTTGGTATCGTGGAAGG
GAPDH_rev	GCCATCACGCCACAGTTTC
Oct4_for	GTGTTCAGCCAAAAGACCATCT
Oct4_rev	GGCCTGCATGAGGGTTTCT
Dnmt3l_for	TGAACAAGGAAGACCTGGACG
Dnmt3l_rev	CAGTGCCTGCTCCTTATGGCT
Klf2_for	ACCAAGAGCTCGCACCTAAA
Klf2_rev	GTGGCACTGAAAGGGTCTGT
Klf4_for	CGGACATCAACGACGTGAG
Klf4_rev	GACGCCTTCAGCACGAACT
DPPA3_for	TAGCGAATCTGTTTCCCCTCT
DPPA3_rev	CTGCTGTAAAGCCACTCATCTT
PECAM1_for	AACAGTGTTGACATGAAGAGCC
PECAM1_rev	TGTAAAACAGCACGTCATCCTT
ESRRB_for	ATCAAGTGCGAGTACATGCTC
ESRRB_rev	CGCCTCCGTTTGGTGATCTC

Table 4.2: List of Antibodies and Concentrations Used

Antibody	Source	Catalog Number	Dilution
β-catenin	BD Transduction	#610154	1:200 ICC
pMLC (Thr18/Ser19)	Cell Signaling	#3674	1:200 ICC
pan-ERM	Cell Signaling	#3142	1:400 ICC
Moesin	Cell Signaling	#3146	1:400 ICC
Ezrin	Cell Signaling	#3145	1:400 ICC
SSEA3	Santa Cruz	sc-21703	1:200 ICC
KLF4	Cell Signaling	#4038	1:200 ICC
YAP	Sigma Aldrich	HPA038885	1:400 ICC
TAZ	Sigma Aldrich	HPA039557	1:400 ICC
Oct3/4	Santa Cruz	sc-5279	1:400 ICC
Sox2	Cell Signaling	#3579	1:400 ICC

Chapter 5 – Appendices

Appendix A: JCAD and Naïve Pluripotency

Done in collaboration Kyle Jacobs.

Introduction: JCAD, Coronary Artery Disease, and Hippo Signaling

Junctional Protein Associated with Coronary Artery Disease (JCAD) is an understudied protein which was first described in genome-wide association study that identified JCAD polymorphisms with linkage disequilibrium to risk for coronary artery disease (Erdmann et al., 2011; Peden et al., 2011). JCAD localizes to cell junctions, contains a 13 amino acid homology to ROCK1, Rho-GDI1, and cingulin, but has no known conserved functional domains. The function of JCAD remains poorly understood, with JCAD's only suggested role being in negative regulation of Hippo signaling (Jones et al., 2018; Ye et al., 2017). The JCAD mouse ortholog is expressed in endothelium in development and germline knockout disrupts vascular homeostasis (Visel et al., 2004). Expression of the JCAD mouse ortholog has also been detected in naïve mouse embryonic stem cells (ESCs), with knockout of TAp73 leading to loss of JCAD expression (López-Ferreras et al., 2021). These data suggests that JCAD may serve additional roles in regulation of transcriptional programs regulating cell-cell and cell-matrix adhesions mechanics in addition to Hippo pathway regulation. Given this potential dual-function role in regulation of both Hippo signaling, adhesion mechanics, and detectable expression in naïve murine ESCs, we sought to characterize if JCAD was expressed in naïve human ESCs.

Results: JCAD is enriched at cell-cell junctions and in the nucleus of human naïve embryonic stem cells.

For morphological analysis, HUES8 primed hESCs were grown on Matrigel and dedifferentiated to naïve pluripotency using previously reported conditions in an mTeSR-based medium supplemented with ERK (PD0325901) and GSK3 (CHIR99021) inhibitors, the adenylyl cyclase activator forskolin, human leukemia inhibitory factor (LIF), basic fibroblast growth factor (bFGF), and ascorbic acid (Duggal et al., 2015; Qin et al., 2016). Colonies of cells were fixed, immunolabeled for JCAD (Sigma Aldrich, #HPA017956, 1:200), and stained with phalloidin. Phalloidin staining confirmed the presence of a supracellular actin ring, which was inhibited with addition of CK666 (**Figure 5.1**). JCAD immunolabeling revealed prominent localization at cell-cell junctions in naïve colonies (**Figure 5.1, yellow arrows**). This was absent in both primed colonies and colonies differentiated in the presence of CK666. Additionally, we observed an increased in nuclear JCAD localization in naïve controls which was not mitigated with addition of CK666 (**Figure 5.1, bottom row**).

Discussion and Future Directions

To investigate the possibility of JCAD contributing to the regulation of the differences in Hippo signaling and cell-cell adhesion we observed upon transition to naïve pluripotency, we interrogated the expression and localization of JCAD in primed, naïve, and CK666-treated hESC colonies. We found that the naïve state correlated with prominent localization of JCAD both at cell-cell junctions as well as in the nucleus. JCAD

has been shown to mediate both cell-cell adhesion and cytoskeletal reorganization in endothelial cells suggesting that JCAD may play a role in maintaining the mechanical strength of endothelial cells (Akashi et al., 2011). The changes in cell-cell adhesion dynamics we observe upon transition to naïve pluripotency may in part be mediated by JCAD. Similarly, the increased junctional signal of JCAD is consistent with previous findings that junctional JCAD negatively regulates Hippo signaling and promotes nuclear YAP localization (Ye et al., 2017). These data suggest that JCAD may function both as a regulator of adhesion and colony mechanics, but also mechanosensitive signaling activity in human naïve ESCs. In the future, it may be worth knocking out JCAD in hESCs and assessing adhesion dynamics, colony mechanics, and Hippo signaling during acquisition of naïve pluripotency.

Localization of JCAD to cell-cell junctions was impaired with the addition of CK666; interestingly, the enriched nuclear localization of JCAD we observed in human naïve ESCs remained with addition of CK666. This suggests that JCAD may still be functioning transcriptionally, although the exact role of nuclear JCAD remains unknown. Cadherins themselves are known to be endogenously regulated during development, occurring as cells exit pluripotency (Bhatt et al., 2013). In mouse, a switch occurs from E-cadherin expression in naïve ESCs to N-cadherin in primed ESCs (Weinberger et al., 2016b). In humans however, naïve ESCs expression both E-cadherin and N-cadherin (Theunissen et al., 2016). Thus cadherin-associated proteins such as JCAD may read out this cadherin code in some capacity, although the specific cadherins JCAD associate with remains unclear. These links between adherens junctional proteins, their associated

binding partners, and the cell interior represent an exciting avenue to understand the molecular mechanisms behind how hESCs respond to mechanical stimulation both *in vitro* and *in vivo*. In the future, comparison studies between naïve hESCs with or without JCAD knockout may help inform the exact role that JCAD plays transcriptionally.

Figures

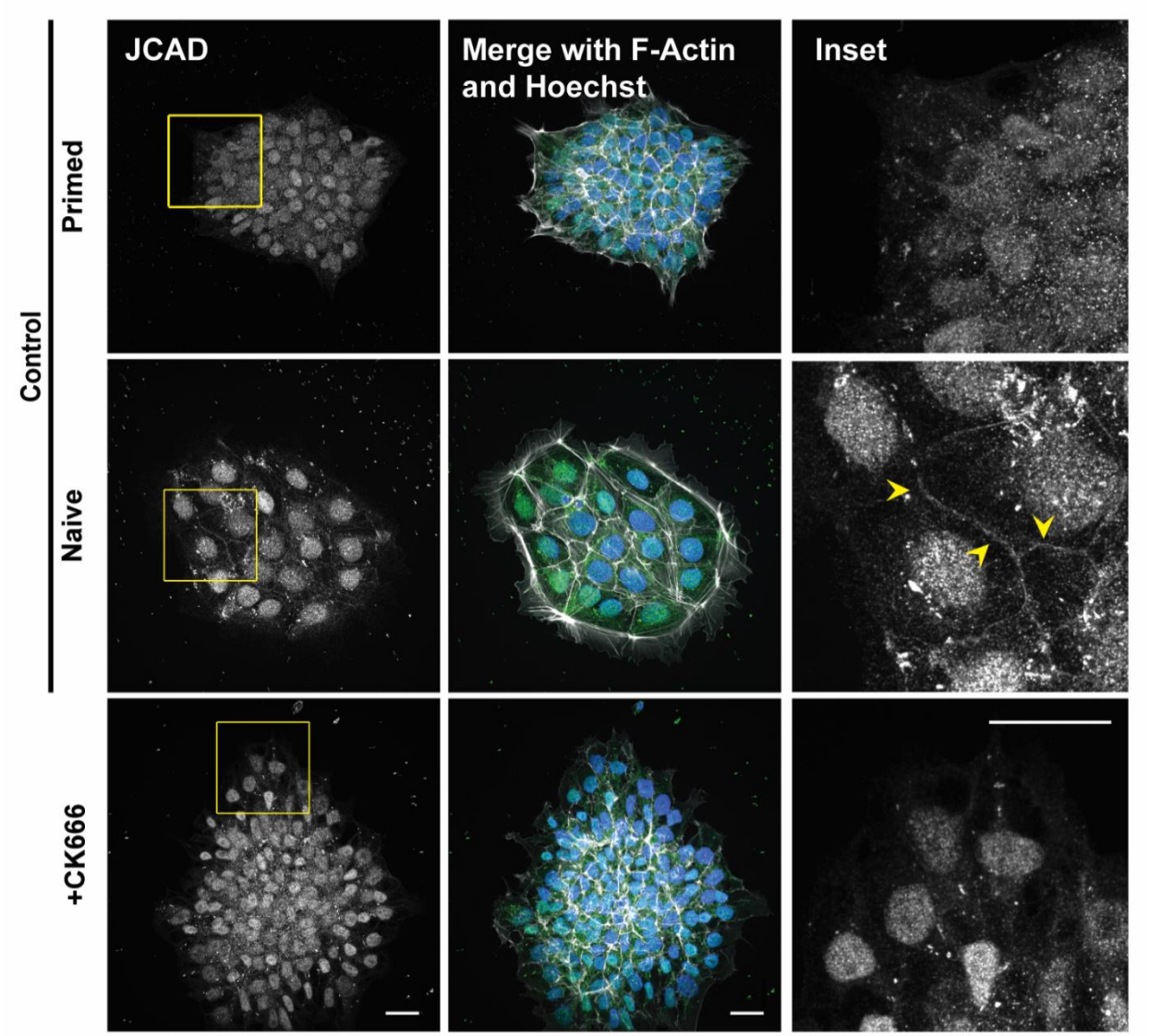

Figure 5.1: JCAD localizes to cell-cell junctions and is enriched in the nucleus of naïve hESCs.

Confocal images of D6 naïve hESCs maintained in the absence (control) or presence of 80 µM CK666 and immunolabeled for JCAD, stained for F-actin with phalloidin and nuclei with Hoechst. Inset panels are magnifications of yellow boxes. Yellow arrows indicate JCAD localizing to cell-cell junctions. Scale bars, 25 µM.

Chapter 6 – Discussion

Discussion and Future Directions

Understanding the cell biology of embryonic stem cells, including how cell fate decisions are made, how differentiation occurs, and what regulates these decisions, is essential for our understanding of developmental biology and can contribute to approaches in regenerative medicine. Pluripotent stem cells (PSCs) are capable of self-renewal and differentiation into any cell type of the body, thus making them the ideal source of cells for therapeutic regenerative interventions. To capitalize on the resource, research within the field has primarily focused on the role of transcription factors and how to regulate their activity in order to guide PSCs to specific cell fates. Despite this focus, the endogenous mechanisms which regulate these transcription factors, pathways, and stimuli which activate them remain poorly understood. A profound and consistent change in cellular morphology occurs when cells exit the pluripotent state and progress down lineages towards a terminal cell fate, yet how the cytoskeleton and cytoskeletal dynamics regulate human PSCs remains unknown.

The main focus of my thesis work resolved a previously unrecognized critical role for Arp2/3 complex activity for the dedifferentiation of primed hESCs to a naïve state of pluripotency that is mediated in part by enabling the nuclear translocation of Hippo pathway effectors YAP and TAZ. This work highlights key fundamental differences between human and mouse PSCs which stresses the need for context and species-specific study. For example, although PSCs from both species undergo profound morphological changes during differentiation and changes in cell fate, only human PSCs are responsive to mechanical stimuli in both the naïve and primed pluripotent states. This

difference may explain why specific mechanosensitive signaling pathways such as Hippo signaling are differentially activated in pre- and post-implantation blastocysts when comparing mouse and human embryos (Gu et al., 2022; Qin et al., 2016). Despite these differences, recent work from our lab also shows Arp2/3 complex activity in mESCs regulates differentiation yet seems to do so via a YAP-independent mechanism (Aloisio & Barber, 2022). Comparisons such as these underscore the importance of using human ESCs for modeling early human development.

In summary, our findings indicate that an actin nucleator and actin cytoskeletal dynamics play a pivotal role in regulating naïve pluripotency in hESCs. These data highlight three important questions for future study: **(1) What role does Arp2/3 complex activity play in differentiation of naïve hESCs as they exit pluripotency? (2) How does Arp2/3 complex activity interface with traditional differentiation programs? (3) What is the role of Arp2/3 complex activity in native developmental contexts such as in the blastocyst?**

(1) Naïve hESCs provide several practical advantages over primed hESCs for downstream study towards targeted cell lineages including enhanced proliferation, single-cell cloning, and a lack epigenetic marks (L. Sun et al., 2021). This lack of marks led to the assumption that, similar to conventions established in the mouse system, that human naïve ESCs had an unrestricted differentiation potential. However, when the differentiation potential of naïve hESCs was assessed, it was found that they exhibited a bias against mesoderm and endoderm differentiation capacity and a favored ectoderm potential (Lee et al., 2017). This differentiation bias was observed independent of the

culture condition, cell line, or method used to generate naïve hESCs, suggesting the source of this bias lies in a deeper-rooted mechanism beyond just transcriptomic regulation. One possible explanation for this differentiation bias lies in the link between colony and cellular mechanics, Wnt signaling, and cell fate determination. Mechanical forces were found to link to cell fate specification in primed hESCs by biasing BMP4 patterning, junctional release of β-catenin, and altering Wnt signaling – ultimately promoting mesoderm differentiation (Muncie et al., 2020). Given our findings that Arp2/3 complex activity regulates the naïve pluripotent state in part through changes in colony and cellular mechanics, Arp2/3 complex activity might also alter the mechanical responses during differentiation as cells exit the naïve state.

(2) During differentiation, multiple transcription factors are known to cooperate, activate transcription of specific target genes, and alter the cellular phenotype. If Arp2/3 complex activity plays a role in cell fate specification upon exit from pluripotency in humans, we would hypothesize that this would likely be independent of YAP and Hippo signaling. In this work, we identified YAP and TAZ, two transcription factor effectors of Hippo signaling as key regulators of naïve pluripotency in humans. However, when cells exit pluripotency and differentiate, YAP is inhibited suggesting Hippo signaling is not a major determinate of cell fate specification in human ESCs (Lian et al., 2010). Actin nucleators such as the Arp2/3 complex and changes in the cytoskeleton likely play larger roles than regulation of individual transcription factors.

Typically, a single transcription factor is insufficient to alter the cellular phenotype and thus multiple transcription factors working in concert define transcriptional circuits

that regulate cellular identity and differentiation. However, this notion is challenged by certain ‘master’ transcription factors that have been identified which can alter cellular phenotype alone. For example, in part of a global screen of transcription factors in directed differentiations, only 4 out of 90 were individually sufficient to induce neural differentiation (Joung et al., 2023). Although this suggests these transcription factors serve as master regulators of neural differentiation, these targets also play roles in other contexts. For example, one of the four genes, RFX4 is known to regulate ciliogenesis and Shh signaling in the central nervous system (Ashique et al., 2009). How these transcription factor circuits function are highly context-dependent and likely undergo extensive rewiring during and after cells differentiate from one cell type into the next. Actin nucleators and cytoskeletal dynamics likely interface with numerous points of regulation in the detection, transmission, and interpretation of cellular cues. It is possible that Arp2/3 complex activity may alter the context in which traditional transcription factor circuits are activated or repressed by the cell.

(3) Although hESCs represent an attractive model of early human development, there are several key similarities and differences between endogenous blastocysts and the clonal cells used in our study. For example, previous work found that culturing either primed or naive hESCs in 3D facilitates expression of genes associated with actin cytoskeletal remodeling and facilitates dedifferentiation to naïve pluripotency (McKee et al., 2021). How expression of these actin cytoskeletal remodeling genes compares to levels observed in endogenous blastocysts or what their function may be remains unclear. Recently, models to generate a human blastocyst-like structures *in vitro* utilizing human

naïve stem cells were established, which appears analogous to the blastocyst stage. These ‘blastoids’ require inhibition of Hippo, ERK, and TGFBβ to form and efficiently generate the necessary extraembryonic tissues such as trophectoderm (Kagawa et al., 2021; Rivron et al., 2018). These studies specifically highlight YAP and Hippo as key regulators of the formation of human blastocysts both developmentally and in these *in vitro* models, yet the endogenous mechanism responsible for Hippo repression and YAP translocation to the nucleus remains unknown. It may be possible that cytoskeletal remodeling and Arp2/3 complex activity is responsible for how these cells interact with their 3D environments.

Understanding differences between naive and primed pluripotency and how these states correlate with *in vivo* development is crucial for the future of regenerative medicine. Multiple studies have demonstrated that naïve PSCs have less biased differentiation potential than primed PSCs, higher targeted differentiation efficiency, and that protocols utilizing naïve PSCs are more reproducible (Lee et al., 2017). Understanding the molecular mechanisms and regulatory systems of naive and primed pluripotency can help to optimize the differentiation of PSCs into specific cell types, enabling the development of more effective cell-based therapies for human diseases.

References

Akashi, M., Higashi, T., Masuda, S., Komori, T., & Furuse, M. (2011). A coronary artery disease-associated gene product, JCAD/KIAA1462, is a novel component of endothelial cell–cell junctions. *Biochemical and Biophysical Research Communications*, *413*(2), 224–229. https://doi.org/10.1016/J.BBRC.2011.08.073

Aloisio, F. M., & Barber, D. L. (2022). Arp2/3 complex activity is necessary for mouse ESC differentiation, times formative pluripotency, and enables lineage specification. *Stem Cell Reports*, *17*(6), 1318–1333. https://doi.org/10.1016/J.STEMCR.2022.05.002

Ashique, A. M., Choe, Y., Karlen, M., May, S. R., Phamluong, K., Solloway, M. J., Ericson, J., & Peterson, A. S. (2009). The Rfx4 transcription factor modulates Shh signaling by regional control of ciliogenesis. *Science Signaling*, *2*(95). https://doi.org/10.1126/SCISIGNAL.2000602/SUPPL_FILE/2_RA70_SM.PDF

Azzolin, L., Panciera, T., Soligo, S., Enzo, E., Bicciato, S., Dupont, S., Bresolin, S., Frasson, C., Basso, G., Guzzardo, V., Fassina, A., Cordenonsi, M., & Piccolo, S. (2014). YAP/TAZ Incorporation in the β-Catenin Destruction Complex Orchestrates the Wnt Response. *Cell*, *158*(1), 157–170. https://doi.org/10.1016/j.cell.2014.06.013

Bhatt, T., Rizvi, A., Batta, S. P. R., Kataria, S., & Jamora, C. (2013). Signaling and mechanical roles of E-cadherin. *Cell Communication & Adhesion*, *20*(6), 189–199. https://doi.org/10.3109/15419061.2013.854778

Chalut, K. J., & Paluch, E. K. (2016). The Actin Cortex: A Bridge between Cell Shape and Function. *Developmental Cell*, *38*(6), 571–573. https://doi.org/10.1016/J.DEVCEL.2016.09.011

Chen, C., Zhang, X., Wang, Y., Chen, X., Chen, W., Dan, S., She, S., Hu, W., Dai, J., Hu, J., Cao, Q., Liu, Q., Huang, Y., Qin, B., Kang, B., & Wang, Y. J. (2022). Translational and post-translational control of human naïve versus primed pluripotency. *IScience*, *25*(1). https://doi.org/10.1016/J.ISCI.2021.103645

Chen, E. Y., Tan, C. M., Kou, Y., Duan, Q., Wang, Z., Meirelles, G. v., Clark, N. R., & Ma'ayan, A. (2013). Enrichr: Interactive and collaborative HTML5 gene list enrichment analysis tool. *BMC Bioinformatics*, *14*(1), 1–14. https://doi.org/10.1186/1471-2105-14-128/FIGURES/3

Chen, Q., Shi, J., Tao, Y., & Zernicka-Goetz, M. (2018). Tracing the origin of heterogeneity and symmetry breaking in the early mammalian embryo. *Nature Communications 2018 9:1*, *9*(1), 1–11. https://doi.org/10.1038/s41467-018-04155-2

Chen, Y. F., Li, Y. S. J., Chou, C. H., Chiew, M. Y., Huang, H. Da, Ho, J. H. C., Chien, S., & Lee, O. K. (2020). Control of matrix stiffness promotes endodermal lineage specification by regulating SMAD2/3 via lncRNA LINC00458. *Science Advances*, *6*(6). https://doi.org/10.1126/SCIADV.AAY0264/SUPPL_FILE/AAY0264_SM.PDF

Chhabra, E. S., & Higgs, H. N. (2007). The many faces of actin: matching assembly factors with cellular structures. *Nature Cell Biology 2007 9:10*, *9*(10), 1110–1121. https://doi.org/10.1038/ncb1007-1110

Chung, H., Lee, B.-K., Uprety, N., Shen, W., Lee, J., & Kim, J. (2016). Yap1 is dispensable for self-renewal but required for proper differentiation of mouse embryonic stem (ES) cells. *EMBO Reports*, *17*(4), 519–529. https://doi.org/10.15252/EMBR.201540933

Clark, A. G., Wartlick, O., Salbreux, G., & Paluch, E. K. (2014). Stresses at the Cell Surface during Animal Cell Morphogenesis. *Current Biology*, *24*(10), R484–R494. https://doi.org/10.1016/J.CUB.2014.03.059

Collier, A. J., & Rugg-Gunn, P. J. (2018). Identifying Human Naïve Pluripotent Stem Cells − Evaluating State-Specific Reporter Lines and Cell-Surface Markers. *BioEssays*, *40*(5), 1700239. https://doi.org/10.1002/BIES.201700239

Connelly, J. T., Gautrot, J. E., Trappmann, B., Tan, D. W. M., Donati, G., Huck, W. T. S., & Watt, F. M. (2010). Actin and serum response factor transduce physical cues from the microenvironment to regulate epidermal stem cell fate decisions. *Nature Cell Biology 2010 12:7*, *12*(7), 711–718. https://doi.org/10.1038/ncb2074

de Belly, H., Paluch, E. K., & Chalut, K. J. (2022). Interplay between mechanics and signalling in regulating cell fate. *Nature Reviews Molecular Cell Biology 2022 23:7*, *23*(7), 465–480. https://doi.org/10.1038/s41580-022-00472-z

de Belly, H., Stubb, A., Yanagida, A., Labouesse, C., Jones, P. H., Paluch, E. K., & Chalut, K. J. (2021a). Membrane Tension Gates ERK-Mediated Regulation of Pluripotent Cell Fate. *Cell Stem Cell*, *28*(2), 273. https://doi.org/10.1016/J.STEM.2020.10.018

de Belly, H., Stubb, A., Yanagida, A., Labouesse, C., Jones, P. H., Paluch, E. K., & Chalut, K. J. (2021b). Membrane Tension Gates ERK-Mediated Regulation of Pluripotent Cell Fate. *Cell Stem Cell*, *28*(2), 273-284.e6. https://doi.org/10.1016/J.STEM.2020.10.018

Duggal, G., Warrier, S., Ghimire, S., Broekaert, D., van der Jeught, M., Lierman, S., Deroo, T., Peelman, L., van Soom, A., Cornelissen, R., Menten, B., Mestdagh, P., Vandesompele, J., Roost, M., Slieker, R. C., Heijmans, B. T., Deforce, D., de Sutter, P.,

de Sousa Lopes, S. C., & Heindryckx, B. (2015). Alternative Routes to Induce Naïve Pluripotency in Human Embryonic Stem Cells. *STEM CELLS*, *33*(9), 2686–2698. https://doi.org/10.1002/stem.2071

Erdmann, J., Willenborg, C., Nahrstaedt, J., Preuss, M., König, I. R., Baumert, J., Linsel-Nitschke, P., Gieger, C., Tennstedt, S., Belcredi, P., Aherrahrou, Z., Klopp, N., Loley, C., Stark, K., Hengstenberg, C., Bruse, P., Freyer, J., Wagner, A. K., Medack, A., … Schunkert, H. (2011). Genome-wide association study identifies a new locus for coronary artery disease on chromosome 10p11.23. *European Heart Journal*, *32*(2), 158–168. https://doi.org/10.1093/EURHEARTJ/EHQ405

Estarás, C., Hsu, H. T., Huang, L., & Jones, K. A. (2017). YAP repression of the WNT3 gene controls hESC differentiation along the cardiac mesoderm lineage. *Genes & Development*, *31*(22), 2250–2263. https://doi.org/10.1101/GAD.307512.117

Frum, T., Murphy, T. M., & Ralston, A. (2018). HIPPO signaling resolves embryonic cell fate conflicts during establishment of pluripotency in vivo. *ELife*, *7*. https://doi.org/10.7554/eLife.42298

Furukawa, K. T., Yamashita, K., Sakurai, N., & Ohno, S. (2017). The Epithelial Circumferential Actin Belt Regulates YAP/TAZ through Nucleocytoplasmic Shuttling of Merlin. *Cell Reports*, *20*(6), 1435–1447. https://doi.org/10.1016/j.celrep.2017.07.032

Ganguly, A., Tang, Y., Wang, L., Ladt, K., Loi, J., Dargent, B., Leterrier, C., & Roy, S. (2015). A dynamic formin-dependent deep F-actin network in axons. *The Journal of Cell Biology*, *210*(3), 401–417. https://doi.org/10.1083/JCB.201506110

Gerecht, S., Bettinger, C. J., Zhang, Z., Borenstein, J. T., Vunjak-Novakovic, G., & Langer, R. (2007). The effect of actin disrupting agents on contact guidance of human embryonic stem cells. *Biomaterials*, *28*(28), 4068–4077. https://doi.org/10.1016/J.BIOMATERIALS.2007.05.027

Goley, E. D., & Welch, M. D. (2006). The ARP2/3 complex: an actin nucleator comes of age. *Nature Reviews. Molecular Cell Biology*, *7*(10), 713–726. https://doi.org/10.1038/NRM2026

Gu, B., Bradshaw, B., Zhu, M., Sun, Y., Hopyan, S., & Rossant, J. (2022). Live imaging YAP signalling in mouse embryo development. *Open Biology*, *12*(1). https://doi.org/10.1098/RSOB.210335

Hanna, J., Markoulaki, S., Mitalipova, M., Cheng, A. W., Cassady, J. P., Staerk, J., Carey, B. W., Lengner, C. J., Foreman, R., Love, J., Gao, Q., Kim, J., & Jaenisch, R. (2009). Metastable Pluripotent States in NOD-Mouse-Derived ESCs. *Cell Stem Cell*, *4*(6), 513–524. https://doi.org/10.1016/J.STEM.2009.04.015

Hirate, Y., Hirahara, S., Inoue, K. ichi, Kiyonari, H., Niwa, H., & Sasaki, H. (2015). Par-aPKC-dependent and -independent mechanisms cooperatively control cell polarity, Hippo signaling, and cell positioning in 16-cell stage mouse embryos. *Development, Growth & Differentiation*, *57*(8), 544–556. https://doi.org/10.1111/DGD.12235

Hogrebe, N. J., Augsornworawat, P., Maxwell, K. G., Velazco-Cruz, L., & Millman, J. R. (2020). Targeting the cytoskeleton to direct pancreatic differentiation of human pluripotent stem cells. *Nature Biotechnology 2020 38:4*, *38*(4), 460–470. https://doi.org/10.1038/s41587-020-0430-6

Hoon, J. L., Tan, M. H., & Koh, C. G. (2016). The Regulation of Cellular Responses to Mechanical Cues by Rho GTPases. *Cells*, *5*(2). https://doi.org/10.3390/CELLS5020017

Hsiao, C., Lampe, M., Nillasithanukroh, S., Han, W., Lian, X., & Palecek, S. P. (2016a). Human pluripotent stem cell culture density modulates YAP signaling. *Biotechnology Journal*, *11*(5), 662–675. https://doi.org/10.1002/BIOT.201500374

Hsiao, C., Lampe, M., Nillasithanukroh, S., Han, W., Lian, X., & Palecek, S. P. (2016b). Human pluripotent stem cell culture density modulates YAP signaling. *Biotechnology Journal*, *11*(5), 662. https://doi.org/10.1002/BIOT.201500374

Ireland, R. G., & Simmons, C. A. (2015). Human Pluripotent Stem Cell Mechanobiology: Manipulating the Biophysical Microenvironment for Regenerative Medicine and Tissue Engineering Applications. *Stem Cells (Dayton, Ohio)*, *33*(11), 3187–3196. https://doi.org/10.1002/STEM.2105

Janmey, P. A., & McCulloch, C. A. (2007). Cell Mechanics: Integrating Cell Responses to Mechanical Stimuli. *Annual Review of Biomedical Engineering*, *9*(1), 1–34. https://doi.org/10.1146/annurev.bioeng.9.060906.151927

Jones, P. D., Kaiser, M. A., Najafabadi, M. G., Koplev, S., Zhao, Y., Douglas, G., Kyriakou, T., Andrews, S., Rajmohan, R., Watkins, H., Channon, K. M., Ye, S., Yang, X., Björkegren, J. L. M., Samani, N. J., & Webb, T. R. (2018). JCAD, a Gene at the 10p11 Coronary Artery Disease Locus, Regulates Hippo Signaling in Endothelial Cells. *Arteriosclerosis, Thrombosis, and Vascular Biology*, *38*(8), 1711–1722. https://doi.org/10.1161/ATVBAHA.118.310976

Joung, J., Ma, S., Tay, T., Geiger-Schuller, K. R., Kirchgatterer, P. C., Verdine, V. K., Guo, B., Arias-Garcia, M. A., Allen, W. E., Singh, A., Kuksenko, O., Abudayyeh, O. O., Gootenberg, J. S., Fu, Z., Macrae, R. K., Buenrostro, J. D., Regev, A., & Zhang, F. (2023). A transcription factor atlas of directed differentiation. *Cell*, *186*(1), 209-229.e26. https://doi.org/10.1016/J.CELL.2022.11.026

Kagawa, H., Javali, A., Khoei, H. H., Sommer, T. M., Sestini, G., Novatchkova, M., Scholte op Reimer, Y., Castel, G., Bruneau, A., Maenhoudt, N., Lammers, J., Loubersac, S., Freour, T., Vankelecom, H., David, L., & Rivron, N. (2021). Human blastoids model blastocyst development and implantation. *Nature 2021 601:7894*, *601*(7894), 600–605. https://doi.org/10.1038/s41586-021-04267-8

Keung, A. J., Asuri, P., Kumarz, S., & Schaffer8, D. V. (2012). Soft microenvironments promote the early neurogenic differentiation but not self-renewal of human pluripotent stem cellsw. *This Journal Is c The Royal Society of Chemistry*, *4*, 1049–1058. https://doi.org/10.1039/c2ib20083j

Kim, Y., Jang, H., Seo, K., Kim, J. H., Lee, B., Cho, H. M., Kim, H. J., Yang, E., Kim, H., Gim, J. A., Park, Y., Ryu, J. R., & Sun, W. (2022). Cell position within human pluripotent stem cell colonies determines apical specialization via an actin cytoskeleton-based mechanism. *Stem Cell Reports*, *17*(1), 68–81. https://doi.org/10.1016/J.STEMCR.2021.11.005

Kuleshov, M. v., Jones, M. R., Rouillard, A. D., Fernandez, N. F., Duan, Q., Wang, Z., Koplev, S., Jenkins, S. L., Jagodnik, K. M., Lachmann, A., McDermott, M. G., Monteiro, C. D., Gundersen, G. W., & Maayan, A. (2016). Enrichr: a comprehensive gene set

enrichment analysis web server 2016 update. *Nucleic Acids Research*, *44*(W1), W90–W97. https://doi.org/10.1093/NAR/GKW377

Kunath, T., Saba-El-Leil, M. K., Almousailleakh, M., Wray, J., Meloche, S., & Smith, A. (2007). FGF stimulation of the Erk1/2 signalling cascade triggers transition of pluripotent embryonic stem cells from self-renewal to lineage commitment. *Development*, *134*(16), 2895–2902. https://doi.org/10.1242/DEV.02880

Lee, J.-H., Laronde, S., Collins, T. J., Shapovalova, Z., Tanasijevic, B., McNicol, J. D., Fiebig-Comyn, A., Benoit, Y. D., Lee, J. B., Mitchell, R. R., & Bhatia, M. (2017). Lineage-Specific Differentiation Is Influenced by State of Human Pluripotency. *Cell Reports*, *19*(1), 20–35. https://doi.org/10.1016/J.CELREP.2017.03.036

Li, M., & Belmonte, J. C. I. (2017). Ground rules of the pluripotency gene regulatory network. *Nature Reviews. Genetics*, *18*(3), 180–191. https://doi.org/10.1038/NRG.2016.156

Lian, I., Kim, J., Okazawa, H., Zhao, J., Zhao, B., Yu, J., Chinnaiyan, A., Israel, M. A., Goldstein, L. S. B., Abujarour, R., Ding, S., & Guan, K.-L. (2010). The role of YAP transcription coactivator in regulating stem cell self-renewal and differentiation. *Genes & Development*, *24*(11), 1106–1118. https://doi.org/10.1101/gad.1903310

Liu, X., Nefzger, C. M., Rossello, F. J., Chen, J., Knaupp, A. S., Firas, J., Ford, E., Pflueger, J., Paynter, J. M., Chy, H. S., O'Brien, C. M., Huang, C., Mishra, K., Hodgson-Garms, M., Jansz, N., Williams, S. M., Blewitt, M. E., Nilsson, S. K., Schittenhelm, R. B., … Polo, J. M. (2017). Comprehensive characterization of distinct states of human naive pluripotency generated by reprogramming. *Nature Methods 2017 14:11*, *14*(11), 1055–1062. https://doi.org/10.1038/nmeth.4436

López-Ferreras, L., Martínez-García, N., Maeso-Alonso, L., Martín-López, M., Díez-Matilla, Á., Villoch-Fernandez, J., Alonso-Olivares, H., Marques, M. M., & Marin, M. C. (2021). Deciphering the nature of trp73 isoforms in mouse embryonic stem cell models: Generation of isoform-specific deficient cell lines using the crispr/cas9 gene editing system. *Cancers*, *13*(13), 3182. https://doi.org/10.3390/CANCERS13133182/S1

Mair, B., Tomic, J., Masud, S. N., Tonge, P., Weiss, A., Usaj, M., Tong, A. H. Y., Kwan, J. J., Brown, K. R., Titus, E., Atkins, M., Chan, K. S. K., Munsie, L., Habsid, A., Han, H., Kennedy, M., Cohen, B., Keller, G., & Moffat, J. (2019). Essential Gene Profiles for Human Pluripotent Stem Cells Identify Uncharacterized Genes and Substrate Dependencies. *Cell Reports*, *27*(2), 599-615.e12. https://doi.org/10.1016/J.CELREP.2019.02.041

Maître, J. L., Turlier, H., Illukkumbura, R., Eismann, B., Niwayama, R., Nédélec, F., & Hiiragi, T. (2016). Asymmetric division of contractile domains couples cell positioning and fate specification. *Nature 2016 536:7616*, *536*(7616), 344–348. https://doi.org/10.1038/nature18958

Masui, S., Nakatake, Y., Toyooka, Y., Shimosato, D., Yagi, R., Takahashi, K., Okochi, H., Okuda, A., Matoba, R., Sharov, A. A., Ko, M. S. H., & Niwa, H. (2007). Pluripotency governed by Sox2 via regulation of Oct3/4 expression in mouse embryonic stem cells. *Nature Cell Biology*, *9*(6), 625–635. https://doi.org/10.1038/NCB1589

May, R. C. (2001). The Arp2/3 complex: a central regulator of the actin cytoskeleton. *Cellular and Molecular Life Sciences : CMLS*, *58*(11), 1607–1626. https://doi.org/10.1007/PL00000800

McKee, C., Brown, C., Bakshi, S., Walker, K., Govind, C. K., & Rasul Chaudhry, G. (2021). Transcriptomic Analysis of Naïve Human Embryonic Stem Cells Cultured in Three-Dimensional PEG Scaffolds. *Biomoleculles*, *11*(1), 1–21. https://doi.org/10.3390/BIOM11010021

McKee, C., Brown, C., & Chaudhry, G. R. (2019). Self-Assembling Scaffolds Supported Long-Term Growth of Human Primed Embryonic Stem Cells and Upregulated Core and Naïve Pluripotent Markers. *Cells*, *8*(12). https://doi.org/10.3390/CELLS8121650

Mertz, A. F., Che, Y., Banerjee, S., Goldstein, J. M., Rosowski, K. A., Revilla, S. F., Niessen, C. M., Marchetti, M. C., Dufresne, E. R., & Horsley, V. (2013). Cadherin-based intercellular adhesions organize epithelial cell-matrix traction forces. *Proceedings of the National Academy of Sciences of the United States of America*, *110*(3), 842–847. https://doi.org/10.1073/PNAS.1217279110/SUPPL_FILE/SM01.AVI

Messmer, T., von Meyenn, F., Savino, A., Santos, F., Mohammed, H., Lun, A. T. L., Marioni, J. C., & Reik, W. (2019). Transcriptional Heterogeneity in Naive and Primed Human Pluripotent Stem Cells at Single-Cell Resolution. *Cell Reports*, *26*(4), 815. https://doi.org/10.1016/J.CELREP.2018.12.099

Mo, J.-S., Park, H. W., & Guan, K.-L. (2014). The Hippo signaling pathway in stem cell biology and cancer. *EMBO Reports*, *15*(6), 642–656. https://doi.org/10.15252/embr.201438638

Muncie, J. M., Ayad, N. M. E., Lakins, J. N., Xue, X., Fu, J., & Weaver, V. M. (2020). Mechanical Tension Promotes Formation of Gastrulation-like Nodes and Patterns

Mesoderm Specification in Human Embryonic Stem Cells. *Developmental Cell*, *55*(6), 679-694.e11. https://doi.org/10.1016/J.DEVCEL.2020.10.015

Murray, P., Prewitz, M., Hopp, I., Wells, N., Zhang, H., Cooper, A., Parry, K. L., Short, R., Antoine, D. J., & Edgar, D. (2013). The self-renewal of mouse embryonic stem cells is regulated by cell-substratum adhesion and cell spreading. *International Journal of Biochemistry and Cell Biology*, *45*(11), 2698–2705. https://doi.org/10.1016/J.BIOCEL.2013.07.001

Nakamura, T., Okamoto, I., Sasaki, K., Yabuta, Y., Iwatani, C., Tsuchiya, H., Seita, Y., Nakamura, S., Yamamoto, T., & Saitou, M. (2016). A developmental coordinate of pluripotency among mice, monkeys and humans. *Nature*, *537*(7618), 57–62. https://doi.org/10.1038/NATURE19096

Naqvi, S. M., & McNamara, L. M. (2020). Stem Cell Mechanobiology and the Role of Biomaterials in Governing Mechanotransduction and Matrix Production for Tissue Regeneration. *Frontiers in Bioengineering and Biotechnology*, *8*, 1375. https://doi.org/10.3389/FBIOE.2020.597661/BIBTEX

Närvä, E., Stubb, A., Guzmán, C., Blomqvist, M., Balboa, D., Lerche, M., Saari, M., Otonkoski, T., & Ivaska, J. (2017). A Strong Contractile Actin Fence and Large Adhesions Direct Human Pluripotent Colony Morphology and Adhesion. *Stem Cell Reports*, *9*(1), 67–76. https://doi.org/10.1016/J.STEMCR.2017.05.021

Nett, I. R., Mulas, C., Gatto, L., Lilley, K. S., & Smith, A. (2018). Negative feedback via RSK modulates Erk-dependent progression from naïve pluripotency. *EMBO Reports*, *19*(8), e45642. https://doi.org/10.15252/EMBR.201745642

Ng, H. H., & Surani, M. A. (2011). The transcriptional and signalling networks of pluripotency. *Nature Cell Biology*, *13*(5), 490–496. https://doi.org/10.1038/NCB0511-490

Nichols, J., & Smith, A. (2009). Naive and Primed Pluripotent States. *Cell Stem Cell*, *4*(6), 487–492. https://doi.org/10.1016/J.STEM.2009.05.015

Nishio, M., Goto, H., Suzuki, M., Fujimoto, A., Mimori, K., & Suzuki, A. (2015). The Hippo Signaling Pathway: A Candidate New Drug Target for Malignant Tumors. *Innovative Medicine*, 79–94. https://doi.org/10.1007/978-4-431-55651-0_7

Nishioka, N., Inoue, K., Adachi, K., Kiyonari, H., Ota, M., Ralston, A., Yabuta, N., Hirahara, S., Stephenson, R. O., Ogonuki, N., Makita, R., Kurihara, H., Morin-Kensicki, E. M., Nojima, H., Rossant, J., Nakao, K., Niwa, H., & Sasaki, H. (2009a). The Hippo Signaling Pathway Components Lats and Yap Pattern Tead4 Activity to Distinguish Mouse Trophectoderm from Inner Cell Mass. *Developmental Cell*, *16*(3), 398–410. https://doi.org/10.1016/j.devcel.2009.02.003

Nishioka, N., Inoue, K. ichi, Adachi, K., Kiyonari, H., Ota, M., Ralston, A., Yabuta, N., Hirahara, S., Stephenson, R. O., Ogonuki, N., Makita, R., Kurihara, H., Morin-Kensicki, E. M., Nojima, H., Rossant, J., Nakao, K., Niwa, H., & Sasaki, H. (2009b). The Hippo signaling pathway components Lats and Yap pattern Tead4 activity to distinguish mouse trophectoderm from inner cell mass. *Developmental Cell*, *16*(3), 398–410. https://doi.org/10.1016/J.DEVCEL.2009.02.003

Niwa, H., Miyazaki, J. I., & Smith, A. G. (2000). Quantitative expression of Oct-3/4 defines differentiation, dedifferentiation or self-renewal of ES cells. *Nature Genetics*, *24*(4), 372–376. https://doi.org/10.1038/74199

Nolen, B. J., Tomasevic, N., Russell, A., Pierce, D. W., Jia, Z., McCormick, C. D., Hartman, J., Sakowicz, R., & Pollard, T. D. (2009). Characterization of two classes of small molecule inhibitors of Arp2/3 complex. *Nature*, *460*(7258), 1031. https://doi.org/10.1038/NATURE08231

Ohgushi, M., Minaguchi, M., & Sasai, Y. (2015). Rho-Signaling-Directed YAP/TAZ Activity Underlies the Long-Term Survival and Expansion of Human Embryonic Stem Cells. *Cell Stem Cell*, *17*(4), 448–461. https://doi.org/10.1016/J.STEM.2015.07.009

Pagliari, S., Vinarsky, V., Martino, F., Perestrelo, A. R., Oliver De La Cruz, J., Caluori, G., Vrbsky, J., Mozetic, P., Pompeiano, A., Zancla, A., Ranjani, S. G., Skladal, P., Kytyr, D., Zdráhal, Z., Grassi, G., Sampaolesi, M., Rainer, A., & Forte, G. (2020). YAP–TEAD1 control of cytoskeleton dynamics and intracellular tension guides human pluripotent stem cell mesoderm specification. *Cell Death & Differentiation 2020 28:4*, *28*(4), 1193–1207. https://doi.org/10.1038/s41418-020-00643-5

Pagliari, S., Vinarsky, V., Martino, F., Perestrelo, A. R., Oliver De La Cruz, J., Caluori, G., Vrbsky, J., Mozetic, P., Pompeiano, A., Zancla, A., Ranjani, S. G., Skladal, P., Kytyr, D., Zdráhal, Z., Grassi, G., Sampaolesi, M., Rainer, A., & Forte, G. (2021). YAP-TEAD1 control of cytoskeleton dynamics and intracellular tension guides human pluripotent stem cell mesoderm specification. *Cell Death and Differentiation*, *28*(4), 1193–1207. https://doi.org/10.1038/S41418-020-00643-5

Papalazarou, V., & Machesky, L. M. (2021). The cell pushes back: The Arp2/3 complex is a key orchestrator of cellular responses to environmental forces. *Current Opinion in Cell Biology*, *68*, 37. https://doi.org/10.1016/J.CEB.2020.08.012

Peden, J. F., Hopewell, J. C., Saleheen, D., Chambers, J. C., Hager, J., Soranzo, N., Collins, R., Danesh, J., Elliott, P., Farrall, M., Stirrups, K., Zhang, W., Hamsten, A., Parish, S., Lathrop, M., Watkins, H., Clarke, R., Deloukas, P., Kooner, J. S., … Anand, S. S. (2011). A genome-wide association study in Europeans and South Asians identifies five new loci for coronary artery disease. *Nature Genetics*, *43*(4), 339–346. https://doi.org/10.1038/NG.782

Plouffe, S. W., Lin, K. C., Moore, J. L., Tan, F. E., Ma, S., Ye, Z., Qiu, Y., Ren, B., & Guan, K. L. (2018). The Hippo pathway effector proteins YAP and TAZ have both distinct and overlapping functions in the cell. *The Journal of Biological Chemistry*, *293*(28), 11230–11240. https://doi.org/10.1074/JBC.RA118.002715

Pollard, T. D. (2007). Regulation of Actin Filament Assembly by Arp2/3 Complex and Formins. *Annual Review of Biophysics and Biomolecular Structure*, *36*(1), 451–477. https://doi.org/10.1146/annurev.biophys.35.040405.101936

Przybyla, L., Lakins, J. N., & Weaver, V. M. (2016). Tissue Mechanics Orchestrate Wnt-Dependent Human Embryonic Stem Cell Differentiation. *Cell Stem Cell*, *19*(4), 462–475. https://doi.org/10.1016/J.STEM.2016.06.018

Qin, H., Hejna, M., Liu, Y., Sebastiano, V., Song, J. S., Ramalho, M., & Correspondence, -Santos. (2016). *YAP Induces Human Naive Pluripotency*. https://doi.org/10.1016/j.celrep.2016.02.036

Rivron, N. C., Frias-Aldeguer, J., Vrij, E. J., Boisset, J. C., Korving, J., Vivié, J., Truckenmüller, R. K., van Oudenaarden, A., van Blitterswijk, C. A., & Geijsen, N.

(2018). Blastocyst-like structures generated solely from stem cells. *Nature*, *557*(7703), 106–111. https://doi.org/10.1038/s41586-018-0051-0

Rizvi, S. A., Neidt, E. M., Cui, J., Feiger, Z., Skau, C. T., Gardel, M. L., Kozmin, S. A., & Kovar, D. R. (2009). Identification and characterization of a small molecule inhibitor of formin-mediated actin assembly. *Chemistry & Biology*, *16*(11), 1158–1168. https://doi.org/10.1016/J.CHEMBIOL.2009.10.006

Rosowski, K. A., Mertz, A. F., Norcross, S., Dufresne, E. R., & Horsley, V. (2015a). Edges of human embryonic stem cell colonies display distinct mechanical properties and differentiation potential. *Scientific Reports 2015 5:1*, *5*(1), 1–12. https://doi.org/10.1038/srep14218

Rosowski, K. A., Mertz, A. F., Norcross, S., Dufresne, E. R., & Horsley, V. (2015b). Edges of human embryonic stem cell colonies display distinct mechanical properties and differentiation potential. *Scientific Reports 2015 5:1*, *5*(1), 1–12. https://doi.org/10.1038/srep14218

Rossant, J., & Tam, P. P. L. (2017). New Insights into Early Human Development: Lessons for Stem Cell Derivation and Differentiation. *Cell Stem Cell*, *20*(1), 18–28. https://doi.org/10.1016/J.STEM.2016.12.004

Rostovskaya, M., Stirparo, G. G., & Smith, A. (2019). Capacitation of human naïve pluripotent stem cells for multi-lineage differentiation. *Development (Cambridge)*, *146*(7). https://doi.org/10.1242/DEV.172916/VIDEO-1

Scarpa, E., Szabó, A., Bibonne, A., Theveneau, E., Parsons, M., & Mayor, R. (2015). Cadherin Switch during EMT in Neural Crest Cells Leads to Contact Inhibition of

Locomotion via Repolarization of Forces. *Developmental Cell*, *34*(4), 421–434. https://doi.org/10.1016/J.DEVCEL.2015.06.012

Schindelin, J., Arganda-Carreras, I., Frise, E., Kaynig, V., Longair, M., Pietzsch, T., Preibisch, S., Rueden, C., Saalfeld, S., Schmid, B., Tinevez, J. Y., White, D. J., Hartenstein, V., Eliceiri, K., Tomancak, P., & Cardona, A. (2012). Fiji: an open-source platform for biological-image analysis. *Nature Methods 2012 9:7*, *9*(7), 676–682. https://doi.org/10.1038/nmeth.2019

Shellard, A., Szabó, A., Trepat, X., & Mayor, R. (2018). Supracellular contraction at the rear of neural crest cell groups drives collective chemotaxis. *Science (New York, N.Y.)*, *362*(6412), 339–343. https://doi.org/10.1126/SCIENCE.AAU3301

Singh, A. M., Reynolds, D., Cliff, T., Ohtsuka, S., Mattheyses, A. L., Sun, Y., Menendez, L., Kulik, M., & Dalton, S. (2012). Signaling network crosstalk in human pluripotent cells: a Smad2/3-regulated switch that controls the balance between self-renewal and differentiation. *Cell Stem Cell*, *10*(3), 312–326. https://doi.org/10.1016/J.STEM.2012.01.014

Skamagki, M., Wicher, K. B., Jedrusik, A., Ganguly, S., & Zernicka-Goetz, M. (2013). Asymmetric localization of Cdx2 mRNA during the first cell-fate decision in early mouse development. *Cell Reports*, *3*(2), 442–457. https://doi.org/10.1016/J.CELREP.2013.01.006

Sun, L., Fu, X., Ma, G., & Hutchins, A. P. (2021). Chromatin and Epigenetic Rearrangements in Embryonic Stem Cell Fate Transitions. *Frontiers in Cell and Developmental Biology*, *9*, 174. https://doi.org/10.3389/FCELL.2021.637309/BIBTEX

Sun, Y., Villa-Diaz, L. G., Lam, R. H. W., Chen, W., Krebsbach, P. H., & Fu, J. (2012). Mechanics regulates fate decisions of human embryonic stem cells. *PloS One*, *7*(5). https://doi.org/10.1371/JOURNAL.PONE.0037178

Szczerbinska, I., Gonzales, K. A. U., Cukuroglu, E., Ramli, M. N. bin, Lee, B. P. G., Tan, C. P., Wong, C. K., Rancati, G. I., Liang, H., Göke, J., Ng, H. H., & Chan, Y. S. (2019). A Chemically Defined Feeder-free System for the Establishment and Maintenance of the Human Naive Pluripotent State. *Stem Cell Reports*, *13*(4), 612–626. https://doi.org/10.1016/J.STEMCR.2019.08.005

Takashima, Y., Guo, G., Loos, R., Nichols, J., Ficz, G., Krueger, F., Oxley, D., Santos, F., Clarke, J., Mansfield, W., Reik, W., Bertone, P., & Smith, A. (2014a). Resetting Transcription Factor Control Circuitry toward Ground-State Pluripotency in Human. *Cell*, *158*(6), 1254–1269. https://doi.org/10.1016/J.CELL.2014.08.029

Takashima, Y., Guo, G., Loos, R., Nichols, J., Ficz, G., Krueger, F., Oxley, D., Santos, F., Clarke, J., Mansfield, W., Reik, W., Bertone, P., & Smith, A. (2014b). Resetting Transcription Factor Control Circuitry toward Ground-State Pluripotency in Human. *Cell*, *158*(6), 1254–1269. https://doi.org/10.1016/J.CELL.2014.08.029

Takashima, Y., Guo, G., Loos, R., Nichols, J., Ficz, G., Krueger, F., Oxley, D., Santos, F., Clarke, J., Mansfield, W., Reik, W., Bertone, P., & Smith, A. (2014c). Resetting transcription factor control circuitry toward ground-state pluripotency in human. *Cell*, *158*(6), 1254–1269. https://doi.org/10.1016/J.CELL.2014.08.029/ATTACHMENT/0F14E8E4-AB7C-4C23-A453-B4EFB26A9D7C/MMC4.XLSX

Tatapudy, S., Aloisio, F., Barber, D., & Nystul, T. (2017). Cell fate decisions: emerging roles for metabolic signals and cell morphology. *EMBO Reports*, *18*(12), 2105–2118. https://doi.org/10.15252/embr.201744816

Theunissen, T. W., Friedli, M., Trono, D., Ecker, J. R., & Jaenisch, R. (2016). Molecular Criteria for Defining the Naive Human Pluripotent State. *Cell Stem Cell*, *19*, 502–515. https://doi.org/10.1016/j.stem.2016.06.011

Theunissen, T. W., Powell, B. E., Wang, H., Mitalipova, M., Faddah, D. A., Reddy, J., Fan, Z. P., Maetzel, D., Ganz, K., Shi, L., Lungjangwa, T., Imsoonthornruksa, S., Stelzer, Y., Rangarajan, S., D'Alessio, A., Zhang, J., Gao, Q., Dawlaty, M. M., Young, R. A., … Jaenisch, R. (2014). Systematic Identification of Culture Conditions for Induction and Maintenance of Naive Human Pluripotency. *Cell Stem Cell*, *15*(4), 471–487. https://doi.org/10.1016/J.STEM.2014.07.002

Trusler, O., Huang, Z., Goodwin, J., & Laslett, A. L. (2017). *Cell surface markers for the identification and study of human naive pluripotent stem cells*. https://doi.org/10.1016/j.scr.2017.11.017

Verstreken, C. M., Labouesse, C., Agley, C. C., & Chalut, K. J. (2019). Embryonic stem cells become mechanoresponsive upon exit from ground state of pluripotency. *Open Biology*, *9*(1). https://doi.org/10.1098/RSOB.180203

Vining, K. H., & Mooney, D. J. (2017). Mechanical forces direct stem cell behaviour in development and regeneration. *Nature Reviews. Molecular Cell Biology*, *18*(12), 728–742. https://doi.org/10.1038/nrm.2017.108

Visel, A., Thaller, C., & Eichele, G. (2004). GenePaint.org: an atlas of gene expression patterns in the mouse embryo. *Nucleic Acids Research*, *32*(Database issue), D552. https://doi.org/10.1093/NAR/GKH029

Warrier, S., van der Jeught, M., Duggal, G., Tilleman, L., Sutherland, E., Taelman, J., Popovic, M., Lierman, S., Chuva De Sousa Lopes, S., van Soom, A., Peelman, L., van Nieuwerburgh, F., de Coninck, D. I. M., Menten, B., Mestdagh, P., van de Sompele, J., Deforce, D., de Sutter, P., & Heindryckx, B. (2017). Direct comparison of distinct naive pluripotent states in human embryonic stem cells. *Nature Communications*, *8*, 15055. https://doi.org/10.1038/ncomms15055

Watanabe, S., Umehara, H., Murayama, K., Okabe, M., Kimura, T., & Nakano, T. (2006). Activation of Akt signaling is sufficient to maintain pluripotency in mouse and primate embryonic stem cells. *Oncogene 2006 25:19*, *25*(19), 2697–2707. https://doi.org/10.1038/sj.onc.1209307

Weinberger, L., Ayyash, M., Novershtern, N., & Hanna, J. H. (2016a). Dynamic stem cell states: naive to primed pluripotency in rodents and humans. *Nature Reviews Molecular Cell Biology 2016 17:3*, *17*(3), 155–169. https://doi.org/10.1038/nrm.2015.28

Weinberger, L., Ayyash, M., Novershtern, N., & Hanna, J. H. (2016b). Dynamic stem cell states: naive to primed pluripotency in rodents and humans. *Nature Reviews. Molecular Cell Biology*, *17*(3), 155–169. https://doi.org/10.1038/NRM.2015.28

Wrighton, P. J., Klim, J. R., Hernandez, B. A., Koonce, C. H., Kamp, T. J., & Kiessling, L. L. (2014). Signals from the surface modulate differentiation of human pluripotent stem cells through glycosaminoglycans and integrins. *Proceedings of the National Academy*

of Sciences of the United States of America, *111*(51), 18126–18131. https://doi.org/10.1073/PNAS.1409525111

Xu, Z., Robitaille, A. M., Berndt, J. D., Davidson, K. C., Fischer, K. A., Mathieu, J., Potter, J. C., Ruohola-Baker, H., & Moon, R. T. (2016). Wnt/β-catenin signaling promotes self-renewal and inhibits the primed state transition in naïve human embryonic stem cells. *Proceedings of the National Academy of Sciences of the United States of America*, *113*(42), E6382–E6390. https://doi.org/10.1073/PNAS.1613849113

Yang, Q., Zhang, X. F., Pollard, T. D., & Forscher, P. (2012). Arp2/3 complex–dependent actin networks constrain myosin II function in driving retrograde actin flow. *The Journal of Cell Biology*, *197*(7), 939. https://doi.org/10.1083/JCB.201111052

Ye, J., Li, T. S., Xu, G., Zhao, Y. M., Zhang, N. P., Fan, J., & Wu, J. (2017). JCAD Promotes Progression of Nonalcoholic Steatohepatitis to Liver Cancer by Inhibiting LATS2 Kinase Activity. *Cancer Research*, *77*(19), 5287–5300. https://doi.org/10.1158/0008-5472.CAN-17-0229

Zenker, J., White, M. D., Gasnier, M., Alvarez, Y. D., Lim, H. Y. G., Bissiere, S., Biro, M., & Plachta, N. (2018). Expanding Actin Rings Zipper the Mouse Embryo for Blastocyst Formation. *Cell*, *173*(3), 776-791.e17. https://doi.org/10.1016/J.CELL.2018.02.035

Zhao, B., Li, L., Lu, Q., Wang, L. H., Liu, C. Y., Lei, Q., & Guan, K. L. (2011). Angiomotin is a novel Hippo pathway component that inhibits YAP oncoprotein. *Genes & Development*, *25*(1), 51–63. https://doi.org/10.1101/GAD.2000111

Zhao, B., Wei, X., Li, W., Udan, R. S., Yang, Q., Kim, J., Xie, J., Ikenoue, T., Yu, J., Li, L., Zheng, P., Ye, K., Chinnaiyan, A., Halder, G., Lai, Z. C., & Guan, K. L. (2007).

Inactivation of YAP oncoprotein by the Hippo pathway is involved in cell contact inhibition and tissue growth control. *Genes & Development*, *21*(21), 2747. https://doi.org/10.1101/GAD.1602907

Publishing Agreement

It is the policy of the University to encourage open access and broad distribution of all theses, dissertations, and manuscripts. The Graduate Division will facilitate the distribution of UCSF theses, dissertations, and manuscripts to the UCSF Library for open access and distribution. UCSF will make such theses, dissertations, and manuscripts accessible to the public and will take reasonable steps to preserve these works in perpetuity.

I hereby grant the non-exclusive, perpetual right to The Regents of the University of California to reproduce, publicly display, distribute, preserve, and publish copies of my thesis, dissertation, or manuscript in any form or media, now existing or later derived, including access online for teaching, research, and public service purposes.

DocuSigned by:
Nathaniel Meyer
AB2AC25892EB416...
Author Signature

3/21/2023
Date